# SCIENTIA BRUNEIANA

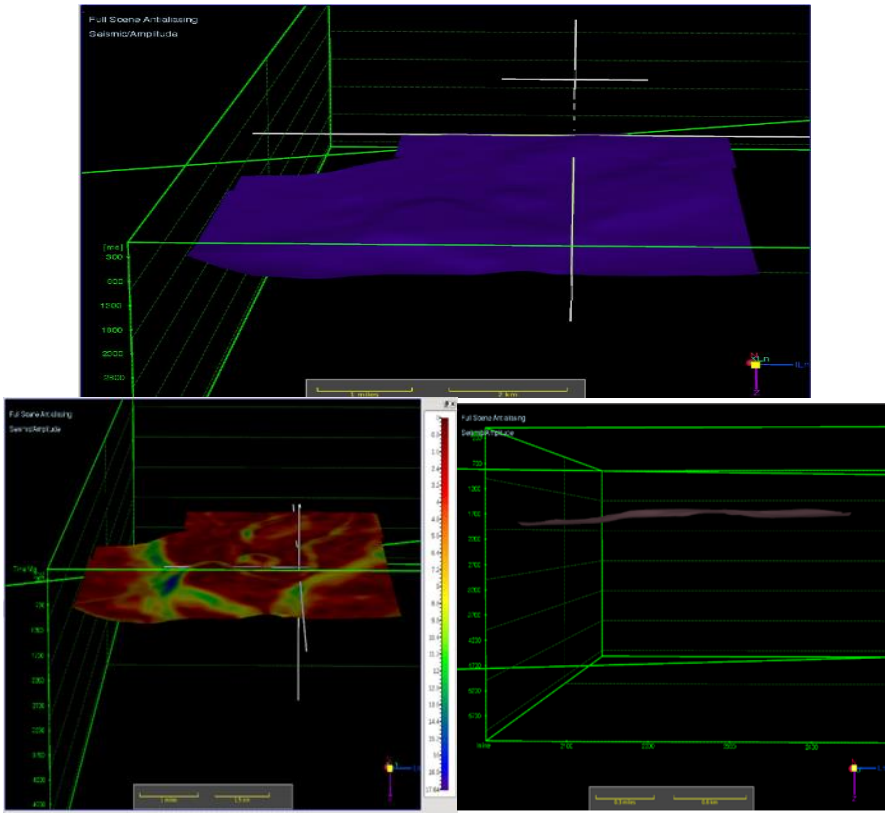

OFFICIAL JOURNAL OF
**THE FACULTY OF SCIENCE**
UNIVERSITI BRUNEI DARUSSALAM

ISSN : 1819-9550 (Print), 2519-9498 (Online) - Volume : 17(1), 2018

First Published 2018 by

Faculty of Science,
Universiti Brunei Darussalam
Jalan Tungku Link
Bandar Seri Begawan BE1410
Brunei Darussalam



This book consists of papers prepared by staff of Universiti Brunei Darussalam and other academic institutions, and peer-reviewed by local and international referees.

---

Cataloguing in Publication Data

---

Scientia Bruneiana / Chief Editor Lim Lee Hoon

47 p. + iv; 30 cm

ISSN 2519-9498 (Online), ISSN 1819-9550 (Print)

1. Research – Brunei Darussalam. 2. Science – Brunei Darussalam

Q180.B7 B788 2018

Cover photos: Horizon map of Field X, Cibulakan Atas formation, West Java Basin. (Courtesy: Ryan Bobby Andika and Haritsari Dewi).

Printed in Brunei Darussalam by
Educational Technology Centre,
Universiti Brunei Darussalam

mk

# SCIENTIA BRUNEIANA
# Vol. 17, No. 1

**Greetings from the Dean of UBD's Faculty of Science.**

I am pleased to introduce the first issue of *Scientia Bruneiana* for 2018, which again showcases the latest findings of local and international researchers in various fields of the biological, physical and mathematical sciences. One of the great strengths of this journal is that it encourages contributions from both the fundamental and applied sciences, thus promoting inter- and multi-disciplinarity.

Universiti Brunei Darussalam has a strong record of ground-breaking scientific research, and the papers featured in this issue illustrate once again the breadth and ingenuity of our research staff as they tackle problems that are central to the national interest, and important to the global scientific community as a whole. I am proud to also note that international researchers appear as authors or co-authors of some of the papers published here, continuing a trend that serves to reinforce the collaborative links between Bruneian and international scientists.

I would like to thank my colleagues in the Faculty of Science, particularly the authors, associate and subject editors for their ongoing support.

**Yours Sincerely**
**Lim Lee Hoon**
**Chief Editor**
**Scientia Bruneiana**

# SCIENTIA BRUNEIANA

A journal of science and science-related matters published twice a year (January-June and July-December) by the Faculty of Science, University Brunei Darussalam. Contributions are welcomed in any area of science, mathematics, medicine or technology. Authors are invited to submit manuscripts to the editor or any other member of the Editorial Board. Further information including instructions for authors can be found in the Notes to Contributors section (the last three pages).

## EDITORIAL BOARD



**SCIENTIA BRUNEIANA** is published by the Faculty of Science,
Universiti Brunei Darussalam, Brunei Darussalam BE 1410

ISSN 2519-9498 (Online), ISSN 1819-9550 (Print)

1. Research – Brunei Darussalam. 2. Science – Brunei Darussalam

Q180.B7 B788 2018

## *SCIENTIA BRUNEIANA*

Publication Ethics Policy

The Editorial Board of *Scientia Bruneiana* is committed to implementing and maintaining the publication standards of a high-quality peer-reviewed scientific journal.

Each manuscript submitted to *Scientia Bruneiana* is examined by a referee with recognised expertise in the manuscript's subject area, and all communications between the referee and the author(s) pass must first through the Editorial Board, so that the identity of the referee remains confidential.

No one will be appointed as the referee of a manuscript if he or she is known to have a potentially compromising relationship with one or more of the authors of the manuscript, as for example in being related through blood or marriage to an author, or in being the research supervisor or research student of an author.

The Editorial Board of *Scientia Bruneiana* makes every effort to ensure that each paper published in the journal is free of plagiarism, redundant or recycled text, and fabricated or misrepresented data. Where possible, plagiarism detection software will be used to check for plagiarised or recycled text.

Provided that a manuscript is free of the ethical lapses described in the previous paragraph, the decision to publish it in *Scientia Bruneiana* is based entirely on its scientific or academic merit, as judged by the referee. The referee's assessment of the merit of the manuscript is final. While a full statement of the reasons behind the referee's decision will be passed on to the author(s), no appeals from the author(s) will be entertained.

Under no circumstances will the referee of a paper published in *Scientia Bruneiana* be credited as one of the authors of the paper, and other papers that have been authored or co-authored by the referee will be admitted to the paper's list of references only after an independent third party with expertise in the area has been consulted to ensure that the citation is of central relevance to the paper.

If a member of the Editorial Board of *Scientia Bruneiana* is listed as an author of a manuscript submitted to *Scientia Bruneiana*, that Board member will play no part whatsoever in the processing of the manuscript.

Where necessary, any corrections or retractions of papers previously published in *Scientia Bruneiana* will be printed in the earliest possible edition of the journal, once the need for a correction or retraction has been drawn to the attention of the Editorial Board.

# SCIENTIA BRUNEIANA VOL. 17, NO. 1

## 2018

**Table of Contents** **Page Numbers**

# Lowland rainforest bat communities of Ulu Temburong National Park with two new records for Brunei Darussalam

*Tegan Murrell[1], Phillip J. Bishop[1], Rodzay Abdul Wahab[2] and T. Ulmar Grafe[3*]*

*[1]Department of Zoology, University of Otago, PO Box 56, 9054 Dunedin, New Zealand*
*[2]Institute of Biodiversity and Environmental Research, Universiti Brunei Darussalam, Jalan Tungku Link, Gadong BE 1410, Brunei Darussalam*
*[3]Environmental and Life Sciences, Faculty of Science, Universiti Brunei Darussalam, Jalan Tungku Link, Gadong BE 1410, Brunei Darussalam*

**corresponding author email: grafe@biozentrum.uni-wuerzburg.de*

**Abstract**

Tropical rainforest ecosystems have high levels of both animal and plant biodiversity with many aspects of their ecology understudied. In particular, extensive research is still required to gather accurate estimates of distribution and abundance of forest-interior bat species in Borneo. Accurate abundance data and further knowledge of individual species' ecology is vital for implementing effective conservation. Bats were captured using a harp trap, set up along established trails and around buildings, at Kuala Belalong Field Studies Centre, Ulu Temburong National Park, Brunei Darussalam between 14$^{th}$-19$^{th}$ January 2018. Ulu Temburong National Park is comprised of pristine primary mixed dipterocarp lowland rainforest that has not been exposed to logging or fragmentation. A total of nine bat species were recorded, with two new records for Brunei, *Miniopterus australis* (Lesser bent-winged bat, N = 1) and *Myotis horsfieldii* (Horsfield's myotis, N = 5). Furthermore, a coincidental sighting of a colony of *Megaderma spasma* roosting on the mangrove island Selirong, in Temburong District is reported here. The bat species captured and encountered in this small-scale study expand our understanding of bat communities in Temburong as well as indicate that current records for the area are far from complete. This affirms the need for further work in building up accurate abundance and diversity estimates, both for Ulu Temburong National Park and Brunei Darussalam.

*Index Terms:* Brunei, Chiroptera, conservation, tropical lowland rainforest, Ulu Temburong

## 1. Introduction

Bats have their highest diversity in the tropics and yet are the most understudied of the Bornean mammalian fauna.[1] Struebig *et al.*[1] reported thirty-six bat species for Brunei with highest diversity in Temburong district locations.

The diversity of bat species can be used to indicate ecosystem health[2] due to their sensitivity to habitat disturbances such as climate change and habitat degradation.[3] In addition, bats are thought to provide important economic and ecological services.[4] This includes pollination and seed dispersal for economically important fruiting plants such as bananas, mangos and durian as well as many keystone rainforest plants. Bats are a key component in conservation through their roles as pollinators and seed dispersers. Their behaviour provides important services in aiding restoration of damaged and fragmented rainforests. These services re-establish and maintain biodiversity of forested areas.[5] Insectivorous bats also act as a pest control species through predation on many small invertebrates.[6]

Global decline in bat species over recent years indicates that conservation and monitoring of bat species is of the utmost importance. With current deforestation rates continuing, it is predicted that

up to 40% of bat species could be extinct by the end of the century.[7] Bat species' inventories in the tropics are far from complete and very little research has been done on the ecological importance of individual species. Compiling accurate inventories of bat species within areas such as the pristine rainforests of Temburong, is vital for assessing species diversity and their conservation needs. Effective conservation efforts for bats are likely to impact rainforest ecosystems as a whole.[7,8]

In Brunei Darussalam, on the northwest coast of Borneo, 54% of the land area is still covered by unlogged forest.[9] The Ulu Temburong National Park is the largest protected area in Brunei (50,000 hectares).[10]

Extensive logging, fragmentation and damage of forests in the Malaysian states of Sabah and Sarawak have impacted species diversity in those areas, emphasising the importance of producing accurate records of species diversity within Brunei. Furthermore, this highlights the importance of future protection for areas such as the Ulu Temburong National Park, were there has been no logging or forest fragmentation.[9]

Here we report on bats captured in the mixed-lowland dipterocarp forest around the Kuala Belalong Field Studies Centre (KBSFC), Ulu Temburong National Park, Brunei, over six trapping nights between the 14$^{th}$ and 19$^{th}$ of January 2018 as well as a bat sighting on the mangrove island of Selirong in April 2018.

## 2. Materials and Methods

Bats were catured using a harp trap placed at strategic locations across the Ashton trail and paths between the KBFSC buildings (N 4° 31', E 115° 08'). Traps were on trails and flight trajectories known to be used by bats based on previous trapping surveys[10] and from observing bat flight patterns around the research centre. Traps were set between 5pm and 8am on the 14$^{th}$-19$^{th}$ January 2018. Harp traps are the most effective and humane method of bat capture within a rainforest environment as there is less risk of entanglement that can occur in other bat trapping methods.[11] The catching bag was removed from the trap during the day to prevent capture of other day-time species.

Captured bats were bagged and processed immediately at KBSFC. Measures of forearm length, tail, ears, tragus and feet were taken to determine individual species. Identification was done using Phillips and Phillips[12] and unpublished keys by Matthew J. Streubig based on Payne and Francis.[13] Morphometric measurements were taken using callipers. Bats were returned to the location where they were captured and were then released.

## 3. Results

From our six trapping nights, there was a total of 17 individuals belonging to nine different species (Fig 1.).

*Myotis horsfieldii* (Horsfield's myotis) was the most abundant bat species encountered. This species, along with *Miniopterus australis* (Lesser bent-winged bat), are new records for Brunei. The five *M. horsfieldii* had moderately long ears each with a tapered forward-bent tragus typical of the genus *Myotis*. Forearm length varied between 35.6-37.5 mm and body mass varied between 6.2-7.3 g distinguishing *M. horsfieldii* from other *Myotis* known to occur on Borneo. Two males and three females were captured. The single *M. australis* was a female with forearm length of 38.0 mm, a body mass of 5.37 g and very dark fur. It showed the distinguishing features of the genus *Miniopterus* with the third finger having a short first phalanx and a very long terminal phalanx as well as having short, rounded ears each with a short blunt tragus. The small body size clearly distinguishes *M. australis* from other bent-winged bats.

Other abundant species were *Hipposideros cervinus* (Fawn roundleaf bat) and *Cynopterus minutus* (Forest short-nosed fruit bat). The majority of bats present at Ulu Temburong were insectivorous bats with *C. minutus* being the only frugivorous species present.

On 22 April, 2018, a small colony of six *Megaderma spasma*, one of them a female with infant, were found roosting midmorning in an abandoned building at Selirong.

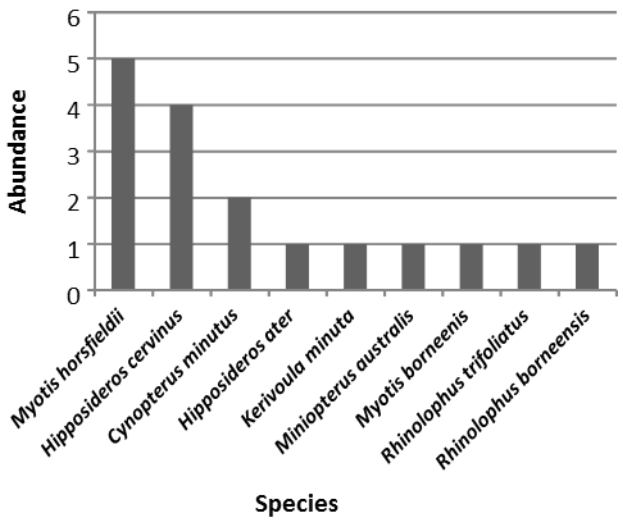


***Figure 1.*** Rank abundance of bat species captured in the harp trap between the 14th-19th January 2018, at KBFSC and along the Ashton trail, Ulu Temburong National Park, Brunei Darussalam. Total number of individuals = 17, from 9 species.

## 4. Discussion

This study captured a total of nine bat species at KBSFC, Ulu Temburong National Park (UTNP), with two new records for Brunei: *Myotis horsfieldii* and *Miniopterus australis*. This brings the total number of bats recorded in Brunei to 65 species.

*M. horsfieldii* is thought to have a wide distribution with broad habitat preferences. It can tolerate some degree of habitat modification. The presence of this species in UTNP is not surprising as it occurs throughout Borneo and other SE Asian countries. They roost in a range of roost types, such as tunnels, caves, palm fronds, building crevices, beams and tree hollows.

*M. australis* is also found throughout Borneo and is tolerant of a broad range of habitats. These bats often roost in very large colonies within caves but have also been known to roost in palm fronds. These bats are seasonal migrants which may account for their appearance in this survey. In addition, this species might have been absent in previous surveys using harp traps set along forest trails because it tends to be an open-space flyer. We suspect that *M. australis* was roosting underneath one of the KBFSC buildings in immediate vicinity to our harp trap.

With the exception of *M. australis*, the bats captured in this study were forest interior bats. Only *C. minutus* was frugivorous. The forests at UTNP have high canopies and the use of harp traps primarily within forest interior trails, accounts for this pattern, as harp traps are biased towards the capture of forest interior bats, such as Hipposideridae and Kerivoulinae[14] which often follow established trails. In contrast, frugivorous bats are commonly canopy foragers[15] and so would not have been captured using a harp trap in the forest interior. Frugivorous bats are also found in higher abundance in disturbed forests, and likely occur in relatively low numbers in the pristine forests of UTNP.[11,16]

A high proportion of the bats recorded were forest-interior, insectivorous bats, with six of the seven species in the data set. These species have been described as sensitive to habitat disturbances.[16] High abundance of these species indicates that there have been low levels of disturbance within UTNP. Previous studies by Struebig *et al.*[8] and Masmin *et al.*[11] also found high diversity of insectivorous bats.

The high canopies and presence of *Kerivoula minuta*, at UTNP further emphasises the pristine nature of the forests. *K. minuta* is sensitive to habitat disturbances due to their preference for roosting in smaller trees (less than 20m).[17] This makes *K. minuta* a good indicator species for the health and quality of forest ecosystems. The presence of this near-threatened species (as listed by the IUCN[18]) suggests that UTNP is an important location for conservation.

The discovery of a colony of the charismatic *Megaderma spasma* on Selirong Island is significant, because only a single individual has

previously been reported from Brunei. This individual was netted in the Peradayan Forest Reserve in Temburong by Struebig *et al.*[1] *M. spasma* is known to roost in tree cavities, caves and abandoned buildings.

This study was a small-scale study, with more trapping nights being required to make accurate diversity estimates. The study was also limited by using a harp trap, which captured mainly forest-interior bats. For accurate data on the presence and abundance of bat species in UTNP further use of multiple traps in a variety of locations would be required. Nevertheless, this diversity snap-shot is informative as it has increased our understanding of the bat communities in this forest.

This study recorded two new species for Brunei Darussalam, *Myotis horsfieldii* and *Miniopterus australis*. The capture of two new records in this small sample and in the case of *M. horsfieldii*, in high abundance, suggests that the bat species inventory for not only UTNP but also Brunei Darussalam is not complete. Brunei supports some of the most diverse bat assemblages in Borneo with approximately two-thirds of the Bornean bat fauna found in Brunei alone.[1] Further surveys should be undertaken to better understand the historical and current processes that shape these rich faunal assemblages.

## 5. Conclusion

This survey adds two new bat species records to both UTNP and Brunei Darussalam. This emphasises the need for further work to compile accurate bat inventories and species abundance data and also the high conservation value of pristine rainforest sites.

## Acknowledgements

We thank the staff at the Kuala Belalong Field Studies Centre, the Universiti Brunei Darussalam, and the University of Otago for facilitating the field work as well as Amy MacIntosh for reviewing the manuscript.

## References

[1] M. J. Struebig, M. Bożek, J. Hildebrand, S. J. Rossiter and D. J. W. Lane, *Biodiversity and Conservation*, **2012**, 21, 3711-3727.
[2] G. Jones, D. S. Jacobs, T. H. Kunz, M. R. Willig and P. A. Racey, *Endangered Species Research*, **2009**, 08, 93-115.
[3] P. Stahlschmidt and C. A. Brühl, *Methods in Ecology and Evolution*, **2012**, 03, 503-508.
[4] T. H. Kunz, E. B. Torrez, D. Bauer, T. Lobova and T. H. Fleming, *Ecology and Conservation Biology*, **2011**, 1223, 1-38.
[5] R. Muscarella and T. H. Fleming, *Biological Reviews*, **2007**, 82, 573-590.
[6] T. C. Wanger, K. Darras, S. Bumrungsri and T. Tscharntke, A.-M. Klein, *Biological Conservation*, **2014,** 171, 220-223.
[7] T. Kingston, *Biodiversity and Conservation*, **2010**, 19, 471-484.
[8] M. J. Struebig, L. Christy, D. Pio and E. Meijaard, *Biodiversity and Conservation*, **2010**, 19, 449-469.
[9] J. E. Bryan, P. L. Shearman, G. P. Asner, D. E. Knapp, G. Aoro and B. Lokes, *PLOS One*, **2013**, 8, e69679.
[10] T. U. Grafe and A. Keller, *Salamandra*, **2009**, 45, 25-38.
[11] H. H. Masmin, K. Collier, P. Sirajuddin and T. U. Grafe, *Scientia Bruneiana*, **2016**, 15, 75-83.
[12] Q. Phillipps and K. Phillipps, *Phillipps' Field Guide to the Mammals of Borneo and Their Ecology: Sabah, Sarawak, Brunei, and Kalimantan*, **2016**, Princeton Field Guides.
[13] J. Payne and C. Francis, *A Field Guide to the Mammals of Borneo*, **2005**, The Sabah Society.
[14] T. Kingston, C.M. Francis, Z. Akbar and T. H. Kunz, *Journal of Tropical Ecology*, **2003**, 19, 67-79.
[15] T. Kingston, B. L. Lim and Z. Akbar, *Bats of Krau Wildlife Reserve*, **2006**, Penerbit Universiti Kebangsaan Malaysia.
[16] I. Castro-Arellano, S. Presley, L. Saldanha, M. Willig and J. Wunderele, *Biological Conservation*, **2007**, 269-285.

[17] G. Kerth, F. Mayer, B. König, *Molecular Ecology*, **2000**, 09, 793-800.
[18] A. M. Hutson, T. Kingston, *Kerivoula minuta*. *The IUCN Red List of Threatened Species*, **2008**, e.T10978A3234174, ver3.1. http://dx.doi.org/10.2305/IUCN.UK.2008.RLTS.T10978A3234174.en [Accessed on 17 March 2018.]

# Checklist of Seedplant holdings of the UBD Herbarium (UBDH), with 234 new plant records for Brunei Darussalam

*Azim Zamri[1] and J.W.F. Slik[1*]*

*[1]Environmental and Life Sciences, Faculty of Science, Universiti Brunei Darussalam, Jalan Tungku Link, Gadong, BE1410, Brunei Darussalam*

**corresponding author email: ferryslik@hotmail.com*

**Abstract**

Here we provide a checklist of all seed plant collections (Angiosperms and Gymnosperms) present in the UBD Herbarium (UBDH). The plants are arranged in alphabetical order by family, genus and species, using the latest taxonomic classifications. UBDH contained a total of 5271 databased seed plant collections (1060 fertile, and 4211 sterile), consisting of 1386 species from 130 families. The collections covered only a limited part of Brunei Darussalam, being concentrated near the easily accessible coastal zones of Muara, Tutong and Belait, as well as near the Kuala Belalong Field Study Centre in Temburong. Because the majority of collections in UBDH came from permanent forest plots, the collections are dominated by tree families, with Dipterocarpaceae both the most collected and species rich family. We found 234 species in UBDH that were not listed in the Brunei checklist and are potentially new records for Brunei Darussalam. This would increase the known number of seed plants in Brunei by ca. 5%. The high number of new species records suggests that the Brunei seed plant flora is still incompletely known.

*Index Terms:* Brunei Darussalam; Brunei checklist; UBDH holdings; new species records; UBD Herbarium; seed plants.

## 1. Introduction

The UBD Herbarium (UBDH) was established in 1994 with the purpose of having a permanent collection of dried plants that allows students and staff to further their research. A detailed description of the UBDH history, aims and future development is provided by Polgar *et al.*[1] The current herbarium has 9862 databased plant specimens, mostly from Brunei Darussalam. Of these, 5271 specimens are seed plants.

The aim of this study was to produce a complete checklist of all seed plant (Gymnosperm and Angiosperm) species present in the UBD herbarium, provide a map with collecting localities, determine the most commonly collected and species rich families, and check for new species records for Brunei Darussalam.

## 2. Materials and Methods

The checklist was based on an existing specimen data base that was available in Microsoft Excel (see ***Figure 1*** and ***Table 1***). This database contained all 9862 specimens stored inside the herbarium cabinets. About 16,000 specimens of trees from Indonesia, 1000 specimens of ferns from China and Sarawak, and several hundred specimens that had not yet been entered into the main collection and data base were not included in the present checklist. Since we focused on seed plants only, algae, bryophytes, lycopods and ferns present in the original database were excluded, leaving 5271 seed plant specimens for the current checklist.

The checklist was organized alphabetically by family and within families alphabetically by genus and species. The classification of the plants followed the latest Angiosperm Phylogeny Group

classification.[2] Synonymy issues were resolved using the The Plant List[3] and the Global Biodiversity Information Facility (GBIF**)**.[4] For each species we extracted the following data from the original specimen data base:

[Family Name]
[Genus] [Species] [Author] [Reference] [Native or Not]
[Local Name] [Growth Form] [Location] [Habitat] [Elevation] [Collection numbers]

**Example:**

**ACANTHACEAE**
***Acanthus ilicifolius* L.** (Sp. Pl. 639 [1753]) [Native]
**Local Name**: Jerudu; **Growth Form**: Small Shrub; **Location**: Brunei-Muara; **Habitat**: Disturbed Mangrove Forest, On Muddy Soils, River Bank and Fringe; **Elevation**: 8 m above seas level (asl); **Collections**: DIBS-5, JOR1.

Not all information for each category (*i.e.* local name, growth form, *etc.*) was present for each species in the data base. In such cases the information was obtained from GBIF[4] and the Brunei checklist.[5] Species that were not identified with certainty (indicated by a question mark in the original data base) were omitted from the checklist. New species observations for Brunei were determined by comparing our checklist with the existing checklist of Brunei.[5] Species not found in the Brunei checklist[5] were considered new species observations. Since many collections in the UBD herbarium are sterile, identifications are all subject to some uncertainty. However, it is important to have this preliminary information available to researchers and government agencies as a working list.

Most specimens were geo-referenced in the original data base, either because the original collectors provided GPS coordinates with their collections, or by using location information provided on the specimen labels in combination with Google Earth Pro[6] to extract the location coordinates. We used this information to create a collection distribution map by superimposing a scatter plot of the collection coordinates on top of a map of Brunei Darussalam.

| | A | B | C | D | E | F |
|---|---|---|---|---|---|---|
| 1 | RecordNo | Family | Genus | Species | Species complete | Author |
| 716 | U/02482 | Asparagaceae | Dracaena | angustifolia | Asparagaceae/Dracaena/Dracaena_angustifolia | Roxb. |
| 717 | U/02483 | Asparagaceae | Dracaena | angustifolia | Asparagaceae/Dracaena/Dracaena_angustifolia | Roxb. |
| 718 | S/00518 | Asparagaceae | Dracaena | angustifolia? | Asparagaceae/Dracaena/Dracaena_angustifolia? | (Medik.) Roxb. |
| 719 | U/00546 | Asparagaceae | Dracaena | elliptica | Asparagaceae/Dracaena/Dracaena_elliptica | Thunb. & Dalm. |
| 720 | U/00547 | Asparagaceae | Dracaena | elliptica | Asparagaceae/Dracaena/Dracaena_elliptica | Thunb. & Dalm. |
| 721 | U/02484 | Asparagaceae | Dracaena | elliptica | Asparagaceae/Dracaena/Dracaena_elliptica | Thunb. |
| 722 | U/02485 | Asparagaceae | Dracaena | elliptica | Asparagaceae/Dracaena/Dracaena_elliptica | Thunb. |
| 723 | S/01010 | Asparagaceae | Dracaena | sp | Asparagaceae/Dracaena/Dracaena_sp | |
| 724 | U/02486 | Asparagaceae | Dracaena | sp | Asparagaceae/Dracaena/Dracaena_sp | |
| 725 | U/02487 | Asparagaceae | Dracaena | sp | Asparagaceae/Dracaena/Dracaena_sp | |
| 726 | U/02488 | Asparagaceae | Dracaena | sp | Asparagaceae/Dracaena/Dracaena_sp | |
| 727 | U/02489 | Asparagaceae | Dracaena | sp | Asparagaceae/Dracaena/Dracaena_sp | |
| 728 | F/00595 | Aspleniaceae | Asplenium | affine | Aspleniaceae/Asplenium/Asplenium_affine | Sw. |
| 729 | F/00607 | Aspleniaceae | Asplenium | affine | Aspleniaceae/Asplenium/Asplenium_affine | Sw. |
| 730 | F/00608 | Aspleniaceae | Asplenium | affine | Aspleniaceae/Asplenium/Asplenium_affine | Sw. |
| 731 | F/00609 | Aspleniaceae | Asplenium | affine | Aspleniaceae/Asplenium/Asplenium_affine | Sw. |
| 732 | F/00623 | Aspleniaceae | Asplenium | macrophyllum | Aspleniaceae/Asplenium/Asplenium_macrophyllum | Sw. |
| 733 | F/00624 | Aspleniaceae | Asplenium | nidus | Aspleniaceae/Asplenium/Asplenium_nidus | L. |
| 734 | F/00625 | Aspleniaceae | Asplenium | nidus | Aspleniaceae/Asplenium/Asplenium_nidus | L. |

***Figure 1.*** The raw Excel database of the plants in UBD Herbarium where ferns (in red text) are excluded and an example of an unconfirmed species indicated in yellow.

## 3. Results and Discussion

A total of 5271 of the 9862 databased collections belonged to seed plants. Of these 1060 were fertile collections mostly collected during botanical surveys, while 4211 were sterile and mostly collected from permanent forest plots.

The collections cover only a limited part of Brunei Darussalam, being concentrated near the easily accessible coastal zones of Muara, Tutong and Belait, as well as near the Kuala Belalong Field Study Centre in Temburong (see ***Figure 2***).

Very few collections have been made in the interior of Brunei.

The 5271 seed plant collections in UBDH consisted of 1386 species belonging to 130 families (see ***Appendix 1***). Most of the species were collected from Temburong and Belait districts (see ***Figure 3***), which is linked to the presence of several permanent forest plots there. Because the majority of collections in UBDH come from permanent forest plots, the collections are dominated by tree families, with Dipterocarpaceae both the most collected and species rich family (see ***Figure 4***).

We found 234 species in UBDH that were not listed in the Brunei checklist[5] (see ***Table 2***). These are potentially new records for Brunei Darussalam. We have to be cautious because a majority of these new records were represented by sterile material, introducing uncertainty in their identification accuracy. If all 234 new species records are confirmed, it would increase the known Brunei seed plant flora by ca. 5%. Despite the uncertainty in species identifications, the high number of new species records does suggest that the Brunei seed plant flora is still incompletely known. As a first step to overcome this, a combined checklist of the holdings of the Brunei National Herbarium (BRUN) and UBDH would form an useful update of the existing Brunei checklist.[5] Furthermore, a coordinated collecting effort, with emphasis on as yet unvisited locations in Brunei, is essential to increase our knowledge of the Brunei seed plant flora.

***Table 1.*** List of information provided in the Excel specimen database.

| **Specimen details** | **Collection details** | **Location** | **Extra details** |
|---|---|---|---|
| Record number | Collector's name | Country | Loan to |
| Family – Genus – Species | Collector number | Province – District – Sub district | Loan date and return date |
| Vernacular name | Collector suffix | Location details | Type status |
| Sublevel category and sublevel name | Collection date | Geology | Duplicate institutes |
| Vegetation type and Habitat | Received date | Altitude | Cabinet store number |
| Species author and reference | Identified by and Identification date | Elevation | Duplication number |
| Uses and plant notes | Previously identified by and identification date | Longitude | Index number |
| Previous family – genus – species name | | Latitude | Picture |


***Figure 2.*** Collection localities of 1183 plant collections present in UBDH.

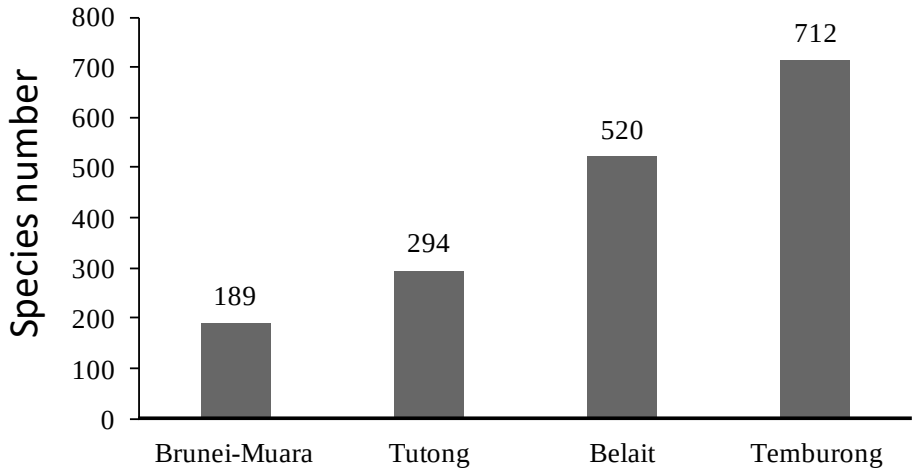


***Figure 3.*** The number of species per district present in the UBDH.

**Acknowledgements**

We would like to thank the following volunteers for their enthusiasm in databasing the 9862 plant collections in UBDH: Dewi Norsaleha Bte Abdulla Duat, Diyana Zafirah Bte Kamis, Hanisha Bte Hashim, Joshua Andrew Maltby-Gander, Noor Anasuha Bte Rosli@Shahrina, Norhaslinda Bte Wasli, Nur Amal Nazira Bte Zaman, Nur Hafidzah Bte Hanafi, Nurhazwani Bte Sirun, Nurul Amirah Bte Ishak/Asahak, Nurul Atiqah Bte Brahim, Nurul Hazlina Bte Zaini, Nuryusreen Ardene Bte Kipli/Zulkifli, and Sumi Yuami. Many UBD staff of the Faculty of Science (FOS) actively contributed at

administrative, technical, and logistical levels. In particular, we wish to thank: Hj Mohd Jamil Bin Dato Hj Abd Hamid (laboratory superintendent), Ong Bee Ling (chief technician), Helen Y. K. Pang (former curatorial assistant), Ting Wei (technician), and Abby Tan (Dean). Thanks also to the UBD Estate Department, for their assistance with maintaining the UBDH infrastructure, and the National Herbarium of Brunei (BRUN) for their help in identifying many of the UBDH plant collections.

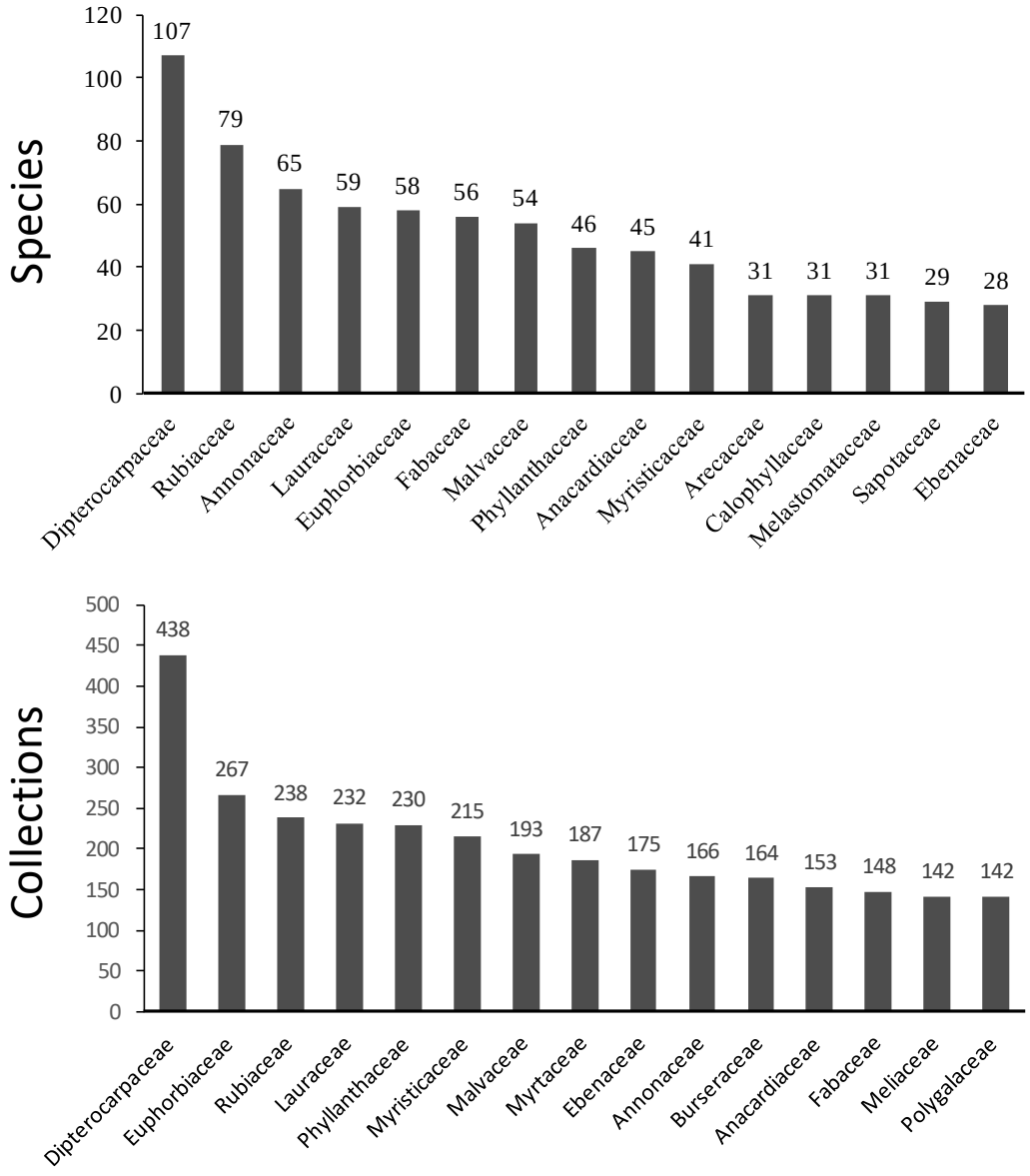


***Figure 4.*** The top 15 most collected and species rich families in the UBDH.

## References

[1] G. Polgar, *et al.*, "The Universiti Brunei Darussalam biological collections: History, present assets, and future development", *Raffles Bulletin of Zoology*, **2018**, 66, 320-336, 2018.

[2] APG-IV, "An update of the Angiosperm Phylogeny Group classification for the orders and families of flowering plants: APG IV", *Botanical Journal of the Linnean Society*, **2016**, 181, 1-20.

[3] "The Plant List, a working list of all plant species", **2013**, version 1.1. http://www.theplantlist.org/ [Accessed 20 April 2018].

[4] "Global Biodiversity Information Facility", **1999**. https://www.gbif.org/ [Accessed 20 April 2018].

[5] M. J. E. Coode *et al.*, "*A checklist of the flowering plants and gymnosperms of Brunei Darussalam*", **1996**, Darusima Trading and Printing Co.

[6] "Google Earth Pro", **2018**, version 7.3.1.4507 (64-bit), Google Incl. https://www.google.com/earth/download/gep/agree.html [Accessed 20 April 2018].

**Appendix 1** (122 pages) has been published as a separate document.

***Table 2.*** Species available in UBDH but absent in BRUN checklist.

| **FAMILY** | **GENUS** |
|---|---|
| ACANTHACEAE | *Clinacanthus nutans* |
| ACHARIACEAE | *Hydnocarpus sumatrana* |
| | *Ryparosa baccaureoides* |
| | *Trichadenia phillipinensis* |
| ACTINIDIACEAE | *Saurauia glabra* |
| | *Saurauia longipetiolata* |
| | *Saurauia subcordata* |
| ANACARDIACEAE | *Buchanania insignis* |
| | *Drimycarpus luridus* |
| | *Gluta macrocarpa* |
| | *Gluta oba* |
| | *Mangifera blommesteinii* |
| | *Mangifera torquenda* |
| | *Melanochyla angustifolia* |
| | *Melanochyla caesia* |
| | *Melanochyla densiflora* |
| | *Melanochyla minutiflora* |
| | *Melanochyla tomentosa* |
| | *Parishia insignis* |
| | *Semecarpus euodiifolius* |
| | *Semecarpus minutipetalus* |
| ANISOPHYLLEACEAE | *Anisophyllea beccariana* |
| ANNONACEAE | *Drepananthus deltoideus* |
| | *Goniothalamus megalocalyx* |
| | *Goniothalamus parallelovenius* |
| | *Goniothalamus roseus* |
| | *Goniothalamus tapisoides* |
| | *Monocarpia euneura* |
| | *Polyalthia bullata* |
| | *Polyalthia obliqua* |
| | *Polyalthia sclerophylla* |
| | *Polyalthia xanthopetala* |
| | *Popowia fusca* |
| | *Popowia hirta* |

| | |
|---|---|
| | *Sageraea sarawakensis* |
| | *Xylopia caudata* |
| | *Xylopia elliptica* |
| APOCYNACEAE | *Alstonia iwahigensis* |
| | *Kibatalia villosa* |
| | *Tabernaemontana divaricata* |
| AQUIFOLIACEAE | *Ilex sclerophylloides* |
| ARACEAE | *Cryptocoryne cordata* |
| ASTERACEAE | *Blumea balsamifera* |
| | *Centratherum punctatum* |
| | *Elephantopus mollis* |
| | *Helianthus annuus* |
| BIGNONIACEAE | *Bignonia corymbosa* |
| BONNETIACEAE | *Ploiarium alternifolium* |
| BURSERACEAE | *Canarium divergens* |
| | *Dacryodes nervosa* |
| CALOPHYLLACEAE | *Calophyllum stipitatum* |
| | *Calophyllum sundaicum* |
| | *Kayea grandis* |
| | *Mesua beccariana* |
| | *Mesua ferrea* |
| CELASTRACEAE | *Euonymus Indicus* |
| | *Lophopetalum pachyphyllum* |
| CHRYSOBALANACEAE | *Atuna nannodes* |
| | *Parinari rigida* |
| CLUSIACEAE | *Garcinia blumei* |
| | *Garcinia brevipes* |
| | *Garcinia caudiculata* |
| | *Garcinia forbesii* |
| | *Garcinia havilandii* |
| | *Garcinia minimiflora* |
| | *Garcinia miquelii* |
| CONVULVULACEAE | *Merremia tridentata* |
| CORNACEAE | *Alangium nobile* |
| | *Mastixia glauca* |
| | *Mastixia macrocarpa* |
| | *Mastixia rostrata* |
| DILLENIACEAE | *Dillenia ovata* |
| | *Dillenia phillippinensis* |
| DIPTEROCARPACEAE | *Hopea dryobalanoides* |
| | *Shorea palembanica* |
| | *Vatica hulletii* |
| EBENACEAE | *Diospyros clementium* |
| | *Diospyros fusiformis* |
| | *Diospyros lanceifolia* |
| | *Diospryos macrophylla* |
| | *Diospyros maritima* |
| | *Diospyros muricata* |
| | *Diospyros oligantha* |

| | |
|---|---|
| | *Diospyros ridleyi* |
| | *Diospyros subrhomboidea* |
| ERIOCAULACEAE | *Eriocaulon sexangulare* |
| ESCALLONIACEAE | *Polyosma borneensis* |
| | *Polyosma kingiana* |
| EUPHORBIACEAE | *Agrostistachys Indica* |
| | *Hevea brasiliensis* |
| | *Jatropha integerrima* |
| | *Macaranga lamellata* |
| | *Macaranga puncticulata* |
| | *Mallotus leucodermis* |
| | *Manihot esculenta* |
| | *Neoscortechinia forbesii* |
| | *Ptychopyxis arborea* |
| | *Ptychopyxis costata* |
| | *Ptychopyxis glochidiifolia* |
| | *Suregada multiflora* |
| | *Trigonostemon capillipes* |
| FABACEAE | *Archidendron jiringa* |
| | *Archidendron triplinervium* |
| | *Crudia reticulata* |
| | *Dialium cochinchinense* |
| | *Dialium patens* |
| | *Dioclea hexandra* |
| | *Flemingia strobilifera* |
| | *Leucaena leucocephala* |
| | *Sindora coriacea* |
| FAGACEAE | *Lithocarpus pusillus* |
| | *Quercus gaharuensis* |
| | *Quercus lineata* |
| GENTIANACEAE | *Utania Spicata* |
| LAMIACEAE | *Clerodendrum japonicum* |
| | *Clerondendrum paniculatum* |
| | *Gmelina arborea* |
| | *Orthosiphon aristatus* |
| | *Teijsmanniodendron sinclairii* |
| LAURACEAE | *Actinodaphne sphaerocarpa* |
| | *Alseodaphne elmeri* |
| | *Alseodaphne longipes* |
| | *Beilschmiedia gemmiflora* |
| | *Beilschmiedia glabra* |
| | *Beilschmiedia lucidula* |
| | *Beilschmiedia wieringae* |
| | *Cinnamomum racemosum* |
| | *Cryptocarya erectinervia* |
| | *Cryptocarya tawaensis* |
| | *Endiandra macrophylla* |
| | *Litsea artocarpifolia* |
| | *Litsea castanea* |

| | |
|---|---|
| | *Litsea caulocarpa* |
| | *Litsea costata* |
| | *Litsea erectinervia* |
| | *Litsea magnifica* |
| | *Phoebe macrophylla* |
| | *Tetranthera angulata* |
| LECYTHIDACEAE | *Barringtonia curranii* |
| LYTHRACEAE | *Lagerstroemia speciosa* |
| MALVACEAE | *Brownlowia ovalis* |
| | *Durio bruneiensis* |
| | *Durio crassipes* |
| | *Durio oxleyanus* |
| | *Heritiera elata* |
| | *Hibiscus rosa-sinensis* |
| | *Microcos latifolia* |
| | *Pentace corneri* |
| | *Pentace rigida* |
| | *Pterospermum diversifolium* |
| | *Pterospermum subpeltatum* |
| | *Scaphium affine* |
| | *Schoutenia accrensens* |
| MELASTOMATACEAE | *Memecylon argenteum* |
| | *Memecylon cantleyi* |
| | *Memecylon longifolium* |
| | *Memecylon megacarpum* |
| | *Pternandra coriacea* |
| | *Pternandra echinata* |
| MELIACEAE | *Aglaia glabrata* |
| | *Aglaia hiernii* |
| | *Aglaia oligophylla* |
| | *Reinwardtiodendron humile* |
| | *Walsura pinnata* |
| MORACEAE | *Artocarpus chama* |
| | *Artocarpus obtusus* |
| | *Prainea frutescens* |
| | *Streblus elongatus* |
| MYRISTICACEAE | *Horsifeldia laticostata* |
| | *Horsfieldia pallidicaula* |
| | *Horsefiedia reticulata* |
| | *Horsfieldia tomentosa* |
| | *Knema conferta* |
| | *Myristica malaccensis* |
| MYRTACEAE | *Syzygium ovalifolium* |
| | *Tristaniopsis beccarii* |
| OCHNACEAE | *Brackenridgea elegantissima* |
| OLACEAE | *Strombosia javanica* |
| OLEACEAE | *Chionanthus cuspidatus* |
| | *Chionanthus havilandii* |
| | *Chionanthus montanus* |

| | |
|---|---|
| OPILIACEAE | *Meliantha suavis* |
| PEDALIACEAE | *Sesamum indicum* |
| PHYLLANTHACEAE | *Aporosa caloneura* |
| | *Aporosa nervosa* |
| | *Baccaurea sarawakensis* |
| | *Cleistanthus hirsutipetalus* |
| | *Sauropus rhamnoides* |
| POACEAE | *Oryza sativa* |
| POLYGALACEAE | *Xanthophyllum eurhynchum* |
| | *Xanthophyllum neglectum* |
| | *Xanthophyllum pauciflorum* |
| | *Xanthophyllum reflexum* |
| | *Xanthophyllum schizocarpon* |
| PRIMULACEAE | *Ardisia hosei* |
| PROTEACEAE | *Helicia symplocoides* |
| | *Heliciopsis velutina* |
| PUTRANJIVACEAE | *Drypetes laevis* |
| | *Drypetes macrostigma* |
| | *Drypetes microphylla* |
| | *Drypetes polyneura* |
| ROSACEAE | *Prunus grisea* |
| RUBIACEAE | *Aidia borneensis* |
| | *Discospermum becarianum* |
| | *Ixora miquelii* |
| | *Morinda lucida* |
| | *Porterandia catappifolia* |
| | *Porterandia grandifolia* |
| | *Tarenna fragrans* |
| RUTACEAE | *Maclurodendron porteri* |
| | *Melicope glabra* |
| | *Micromelum minutum* |
| SALICACEAE | *Casearia tuberculata* |
| | *Homalium longifolium* |
| | *Osmelia maingayi* |
| | *Osmelia philippina* |
| SAPOTACEAE | *Madhuca elmeri* |
| | *Madhuca glabrescens* |
| | *Madhuca kuchingensis* |
| | *Palaquium elegans* |
| | *Palaquium rufolanigerum* |
| | *Payena endertii* |
| | *Payena ferruginea* |
| | *Planchonella maingayi* |
| SIMAROUBACEAE | *Quassia borneensis* |
| STEMONURACEAE | *Gomphandra quadrifida* |
| | *Stemonurus grandifolius* |
| THYMELACEAE | *Aquilaria malaccensis* |
| | *Aquilaria microcarpa* |
| | *Gonystylus calophyllus* |

| | |
|---|---|
| | *Gonystylus forbesii* |
| VERBENACEAE | *Stachytarpheta indica* |
| VIOLACEAE | *Rinorea congesta* |
| ZINGIBERACEAE | *Etlingera coccinea* |

# A fast and sensitive real-time PCR assay to detect *Legionella pneumophila* with the ZEN™ double-quenched probe

*Nur Thaqifah Salihah[1], Mohammad Mosharraf Hossain[2] and Minhaz Uddin Ahmed[1*]*

*[1]Biosensors and Biotechnology Laboratory, Integrated Science Building, Faculty of Science, Universiti Brunei Darussalam, Jalan Tungku Link, Gadong, BE1410, Brunei Darussalam*
*[2]Institute of Forestry and Environmental Sciences, University of Chittagong, Chittagong 4331, Bangladesh*

**corresponding author email: minhaz.ahmed@ubd.edu.bn, minhazua@gmail.com*

**Abstract**

*Legionella pneumophila* is a waterborne pathogen that causes respiratory ailments including Pontiac fever and Legionnaires' disease. A culture-free, fast and sensitive detection technique is very important for detection of the pathogen. The present study describes the implementation of rapid cycle real-time PCR in the detection of *Legionella pneumophila* in water through design and development of a real-time qPCR assay based on the ZEN™ probe chemistry. The assay targeted the *mip* gene for the fast and specific detection of *Legionella pneumophila*. The novel assay was very specific and fast as the amplification was obtained within 30 minutes. Sensitivity of the assay as evaluated in terms of its limit of detection (LoD) was as low as 100 cells/reaction with the quantification range between $1 \times 10^3$ and $1 \times 10^7$ cells/reaction. The assay has been confirmed for repeatability and reproducibility with approximately less than 1% mean intra- and inter-assay variations (CV%). Therefore, the assay reported can be used for a fast, sensitive and specific culture-free detection and quantification of *Legionella pneumophila* in water.

*Index Terms:* Real time PCR, *Legionella pneumophila*, ZEN™ double-quenched probe, Water borne pathogen, Respiratory pathogen

## 1. Introduction

*Legionella pneumophila (L. pneumophila)* – the gram-negative bacterium that naturally occurs as a ubiquitous amoebal parasite in fresh water – may cause sporadic opportunistic infection, mainly in immuno-compromised individuals.[1] The pathogen causes different types of respiratory diseases including an often-fatal pneumonia known as Legionnaires' disease and Pontiac fever.[2] It was first identified as the pathogen that caused the massive outbreak of pneumonia in individuals attending an American Legion convention.[3] Recently, the pathogen has been identified as hosting the largest number of (330+) bacterial effector proteins, which makes it a potential threat to a wide range of hosts including humans.[4]

Conventionally, *L. pneumophila* is detected in water using culture-based methods, which are slow, labor-intensive, costly and create infectious wastes,[5] while giving false negative results due to the fastidious nature of the pathogen. By contrast, real-time PCR provides a faster and more sensitive method of culture-free detection overcoming all these limitations. Real-time PCR has been used to detect and quantify *L. pneumophila* by using TaqMan probes, hybridization probes, molecular beacon probes and EvaGreen dye chemistries.[6-9] However, the minimum time of detection in these assays was 45 minutes.[6]

TaqMan probes are hydrolysis probes with a quencher and a reporter at each end. In its complete form, the TaqMan probe reporter's fluorescence is suppressed by the quencher, but

during PCR amplification the polymerase enzyme hydrolyses the probe that separates the reporter from the quencher, allowing the fluorescence to increase for direct detection of the amplification.

Hybridization probes, on the other hand, are probe systems with two separate oligonucleotides, one with a reporter at the 3'-end and the other with a reporter at the 5'-end. In the annealing step of the PCR amplification, both oligonucleotides anneal to the target sequence, moving the fluorescence reporter and quencher close to each other, and suppressing the fluorescence that allows the detection of the amplification.

Molecular beacons, by contrast, are doubly-labeled hairpin-shaped probe systems. In its hairpin form, the proximity of the reporter and quencher suppresses the fluorescence of the reporter. During amplification, the hairpin structure of the probe opens and hybridizes to the target sequence that separates the reporter from the quencher to allow the detection of the amplification.

Finally, EvaGreen is a double-stranded DNA (dsDNA) binding dye that significantly increases fluorescence upon binding to dsDNA. However, it requires additional post-PCR melting curve analysis, which increases the detection time.

The research reported here takes advantage of recent advancements in real-time PCR thermocycling and detection chemistries to develop a more specific and faster method for detection of the pathogen in water. The 7500 Fast real-time PCR system (Applied Biosystem™ Lifetechnologies, Van Allen Way, U.S.A.) allows rapid cycle amplification and so offers reduced detection time, while the ZEN™ double-quenched hydrolysis probe from IDTDNA, which has an additional internal quencher in between the reporter and quencher, allows for more sensitive and specific detection of target templates.

We also designed novel oligonucleotides based on the highly specific *mip* gene, which encodes a macrophage infectivity potentiator protein virulence factor, to facilitate the entry of the *L. pneumophila* into its hosts,[10,11] thereby enhancing the specificity and selectivity of the assay.

## 2. Materials and Methods

### *2.1 Bacterial strains and quantifications*

The study used genomic DNA purchased from American Type Culture Collection (ATCC, Manassas, U.S.A.) listed in ***Table 1,*** as a reference strain as well as for cross-reactivity analysis**.** The concentration and purity of the genomic DNA were measured in the NanoPhotometer™ P-Class (Implen, München, Germany) spectrophotometer by reading of the absorbance at 260 nm and by calculating the absorbance $A_{260}/A_{280}$ ratio, respectively. The genomic DNAs were then diluted with 1× Tris-EDTA (TE) buffer (10 mM Tris-HCl, 1 mM disodium EDTA, pH 8.0 to appropriate concentrations before use.

***Table 1.*** Genomic DNA of bacteria stains from ATCC.

| Dyes | Stain no./ATCC no. |
|---|---|
| *Legionella pneumophila* | ATCC 33152 |
| *Staphylococcus aureus* | ATCC 25923 |
| *Bacillus cereus* | ATCC 14579 |
| *Bacillus subtilis* | ATCC 23857 |
| *Salmonella enterica* | ATCC 13311 |
| *Escherichia coli* | ATCC 35401 |
| *Clostridium perfringens* | ATCC 13124 |
| *Shigella flexneri* | ATCC 29903 |
| *Campylobacter jejuni* | ATCC 33292 |
| *Yersinia enterocolitica* | ATCC 27739 |
| *Aeromonas hydrophila* | ATCC 7966 |
| *Plesiomonas shigelloides* | ATCC 51903 |
| *Streptococcus pyogens* | ATCC 19615 |
| *Cronobacter sakazakii* | ATCC BAA-894 |
| *Mycobacterium avium* | ATCC BAA-968 |

*2.2 Primer and probe design*

The primer pairs and probes used in this study were designed using the PrimerQuest Tool from Integrated DNA Technologies (IDTDNA, Coralville, U.S.A.) to target a fragment of the *mip* gene of the *L. pneumophila* strain. The primer pairs and probes were designed using sequences of the gene obtained from the GenBank database.[12] The accession number is shown in ***Table 2***.

Primer-Blast[13] was used to confirm the exclusiveness of the primer pairs and probes to *L. pneumophila* strains, while OligoAnalyzer Tool (IDT) assured the absence of strong secondary structures (i.e. primer dimers and hairpin structures) *in-silico*. The primer pair and ZEN™ probe, labeled with the fluorescent dye FAM at the 5'-end, IBFQ quencher at the 3'-end, and an additional internal quencher ZEN™ in the middle of the probe, were purchased from IDTDNA (Singapore Science Park III, Singapore). The oligonucleotides designed and used in this study are listed in ***Table 3***.

*2.3 Fast real-time PCR protocol and amplification condition*

The assay was carried out on the 7500 Fast real-time PCR system (Applied Biosystem™ Lifetechnologies, Van Allen Way, U.S.A.) in a 25 µL PCR mixture that contained Ultrapure MilliQ water, 1× of Buffer II, 500 nM of both the forward and reverse primers, 250 nM of the probe, 1.5 mM $MgCl_2$, 0.2 mM of dNTP mix (Invitrogen™ Lifetechnologies, Van Allen Way, U.S.A.), 0.1× ROX reference dye (Invitrogen™ Life technologies, Van Allen Way, U.S.A.), 0.625U of AmpliTaq DNA polymerase (Applied Biosystem™ Life technologies, Van Allen Way, U.S.A.) and 4 µL of DNA template, and were run in triplicate or duplicate. Rapid cycle amplification was conducted as follows: Initial denaturation at 95° C for 20 seconds, and 40 cycles of denaturation at 95° C for 3 seconds, Annealing/extension for 30 seconds at 60° C. Negative controls were added for each assay. Negative controls replaced DNA templates with Ultrapure MilliQ water.

*2.4 DNA sequencing*

The PCR products of the assay were purified and sequenced by First Base Laboratories (Selangor, Malaysia) to determine the specificity of the assay.

*2.5 Cross-reactivity analysis*

The cross-reactivity of the assay was assessed *in-vitro* with $3 \times 10^6$ fg of genomic DNA of bacterial strains as listed in ***Table 1***.

*2.6 Sensitivity analysis*

The sensitivity of the assay was evaluated by amplifying dilutions of genomic DNA from the *L. pneumophila* reference strain ATCC 3315. The reaction was repeated three times. In the diluted state, 1 cell of *L. pneumophila* was equivalent to approximately 4 fg, calculated from the base pair length of the genomic DNA of the reference strain *L. pneumophila*.[14]

*2.7 Validations of assay performance*

The performance and quantitative capabilities of the assay were evaluated from the amplification curve prepared by using 10-fold serial dilutions of the genomic DNA of *L. pneumophila* ATCC 33152. The range of concentrations of the dilute solutions was $4 \times 10^2$ to $4 \times 10^7$ fg/reaction. The experiments were repeated three times.

***Table 2.*** Accession number and location of target gene.

| Target gene | Accession no. | Locations | References |
|---|---|---|---|
| *mip* | AF095230 | 1-702 | Bumbaugh et al., 2002 |

***Table 3.*** List of designed and selected primer pairs and probes.

| Gene | Name | | Sequence (5'-3') | Locations | Size (bp) |
|---|---|---|---|---|---|
| *mip* | P1mip | F[a]: | ACATCATTAGCTACAGACAAGG | 73-204 | 131 |
| | | P[b]: | 6FAM-AGCATTGGT(ZEN)GCCGATTTGGGAAAG -1BFQ | | |
| | | R[c]: | CCACTCATAGCGTCTTGC | | |

[a]: forward primer sequence

[b]: reverse primer sequence

[c]: probe sequence

## 3. Results and Discussion

### *3.1 Detection time*

In this study, we combined the rapid cycle amplification protocol of 7500 Fast real-time PCR and ZEN™ double-quenched probes to detect *L. pneumophila* in water samples rapidly and reliably. We have chosen the sequence-specific probe-base chemistry (i.e.: the ZEN™ double-quenched probe) to reduce the detection time, as it requires no additional post-amplification melting curve analysis, which could add to the detection time.

The proposed 2-step fast amplification protocol with a fast, real-time PCR instrument reduced the detection time to 30 min, which is significantly faster than conventional culture-based methods that might take up to 10-days,[15] and faster than previously-reported real-time PCR-based methods which use 3-steps standard amplification condition and could take up to 2 hours of amplification time.[6,9,16]

### *3.2 Specificity of the assay*

The specificity of the assay was confirmed with DNA sequencing and cross-reactivity analysis against the bacterial species listed in ***Table 1***. The sequences of PCR products were aligned with the target sequence of *L. pneumophila* ATCC 33152 (accession no. AE017354.1), as shown in ***Figure 1***.

```
Query  866922  ACATCATTAGCTACAGACAAGGATAAGTTGTCTTATAGCATTGGTGCCGATTTGGGGAAG  866981
               ||||||| |||| ||| ||||||||||||||| |||||||||||||| ||| |||||||||
Sbjct  1       ACATCAATAGCGTCAGGCAAGGATAAGTTGTTTGATAGCATTGGTGCAGATATGGGGAAG  60

Query  866982  AATTTTAAAAATCAAGGCATAGATGTTAATCCGGAAGCAATGGCTAAAGGCATGCAAGAC  867041
               ||||||||||||||||||||||||||||||||||||||||||||||||||||||||||||
Sbjct  61      AATTTTAAAAATCAAGGCATAGATGTTAATCCGGAAGCAATGGCTAAAGGCATGCAAGAC  120

Query  867042  GCTATGAGTGG  867052
               ||||||||||||
Sbjct  121     GCTATGAGTGG  131
```

***Figure 1.*** Sequence alignment of PCR products of P1mip ZEN™ probe assays with the sequence of *L. pneumophila* ATCC 33152. Query: sequence of *S. aureus* ATCC 25923; Sbjct: sequence of PCR products.

The results demonstrate that the P1mip assay is quite specific and can amplify target sequences. On the other hand, the cross-reactivity analysis establishes that the proposed assay is highly specific to the target species with no cross-reactivity with other species (***Figure 2A***). This is further confirmed by the gel electrophoresis results, which show only a positive amplification band for the positive controls and none for the other bacterial species (***Figure 2B***).

The overall results of the cross-reactivity analysis for the ZEN™ probe P1mip assay are listed in ***Table 4***. This shows that the P1mip assay is highly specific to the target *L. pneumophila* bacteria, without cross-reactivity with other non-*L. pneumophila* bacterial species.

*3.3 Limit of detection and assay performance*

The sensitivity analysis shows that the P1mip ZEN™ probe assay is able to detect concentrations as low as at 400 fg/reaction or 100 cells/reaction with 77.8% probability. LoD refers to the highest dilutions where observable positive amplification is obtained in the replicates.[17]

Accordingly, the performance of the proposed ZEN™ probe P1mip assay was analyzed by constructing the standard curves and determining the efficiency, the linearity ($R^2$ value), reproducibility and repeatability (intra- and inter-coefficient variations respectively) of each assay under the proposed fast real-time PCR protocol. The standard curves were generated from 10-fold dilutions of *L. pneumophila* ATCC 33152 genomic DNA that yielded DNA solutions with the concentration range $4 \times 10^2$ to $4 \times 10^7$ fg/reaction which was equivalent to $1 \times 10^2$ to $1 \times 10^7$ cell/reaction (see ***Figure 3***).

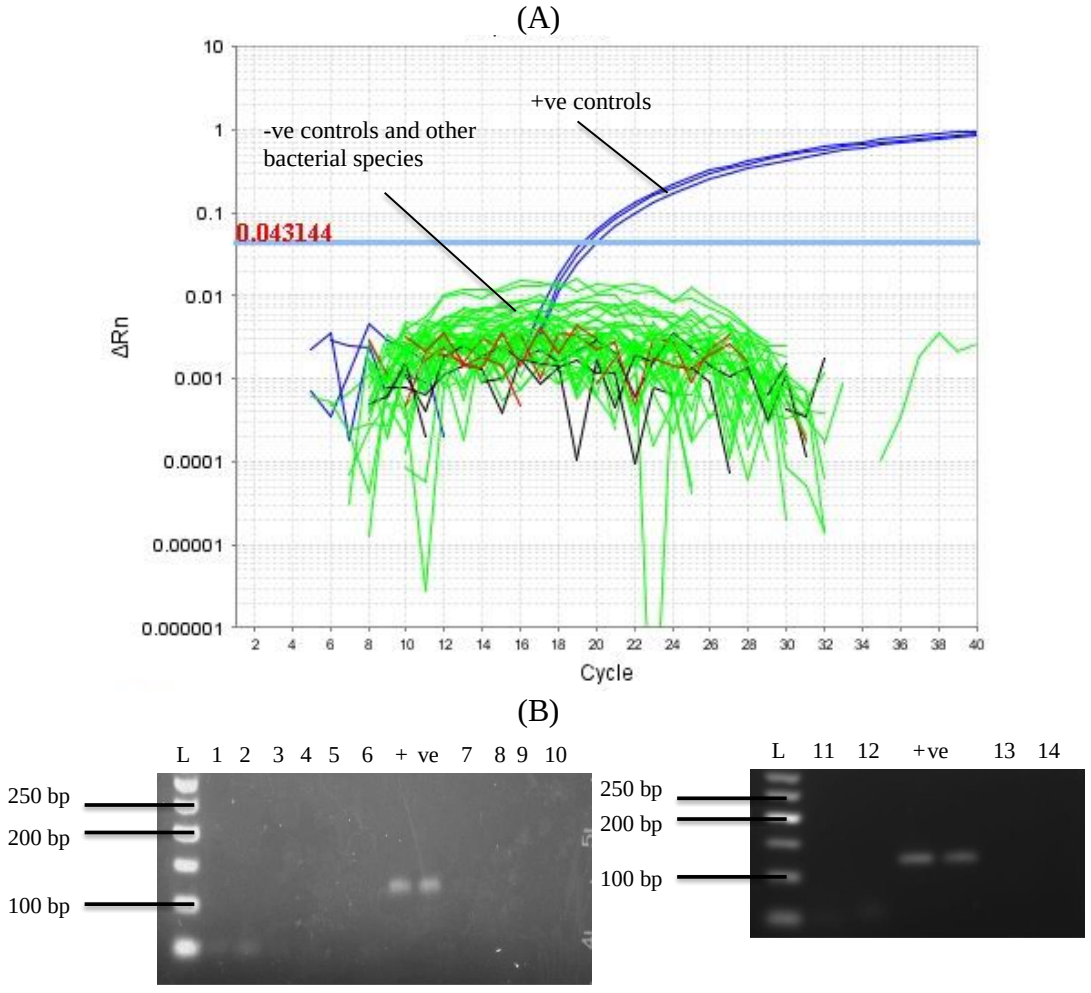


***Figure 2.*** Cross-reactivity analysis for P1mip ZEN™ probe (A) real-time PCR amplification plot; (B) Gel electrophoresis result. (L) 50 bp DNA ladder; (1) *A. hydrophilla;* (2) *B. cereus* (3) *B. subtilis*; (4) *C. jejuni*; (5) *C. perfringens*; (6) *C. sakazakii*; (7) *E. coli*; (8) *M. avium*; (9); *P. shigelloides* (11) *S. flexneri* (12) *S. enterica*; (13) *S. pyogens*; (14) *Y. enterocoalitica*; (+ve) positive control (*L. pneumophila*).

***Table 4.*** Cross-reactivity results of P1mip ZEN™ probe fast real time PCR assays.

| Bacterial species | Cross-reactivity results | Ratio of positive reactions[a] |
|---|---|---|
| | P1mip | P1mip |
| *L. pneumophila* | +[b] | 3/3 |
| *B. cereus* | -[c] | 0/3 |
| *S. aureus* | -[c] | 0/3 |
| *B. subtlis* | -[c] | 0/3 |
| *S. enterica* | -[c] | 0/3 |
| *E. coli* | -[c] | 0/3 |
| *C. perfringens* | -[c] | 0/3 |
| *S. flexneri* | -[c] | 0/3 |
| *C. jejuni* | -[c] | 0/3 |
| *Y. enterocolitica* | -[c] | 0/3 |
| *A. hydrophila* | -[c] | 0/3 |
| *P. shigelloides* | -[c] | 0/3 |
| *S. pyogens* | -[c] | 0/3 |
| *C. sakazakii* | -[c] | 0/3 |
| *M. avium* | -[c] | 0/3 |

[a]: number of positive results per 3 individual reactions

[b]: positive amplifications

[c]: negatuve amplifications

Efficiency was calculated from the standard curve using the equation published by Klein *et al*.[18] The P1mip assays showed an efficiency and linearity (98.923 %; $R^2$=0.996) within the recommended efficiency range and linearity of 90 to 105 % and $R^2$>0.99 for real-time PCR.[19] The assay also produced a linear quantification range (see ***Table 5***) of $1 \times 10^3$ to $1 \times 10^7$ cells/ reaction. The quantification range starts from the highest dilutions with amplifications at >95% probability.[20] It was also highly repeatable, robust, and reproducible and showed approximately less than 1 % mean intra- and inter-assay variation (CV%) (see ***Table 5***). Since the *mip* gene is a single copy gene, the proposed assay can also be used to directly quantify the amount of *L. pneumophila* cell in water samples based on the amount of *mip* gene detected.

## 4. Conclusion

In conclusion, this study has demonstrated that a faster detection of *L. pneumophila* in water samples is possible using a ZEN™ probe fast real-time PCR assay with amplification in 30 min. However, the quantitative capabilities of the proposed assay with other *Legionella* spp. or *L. pneumophila* contaminated water have not yet

been tested. This will be the subject of future research.

**Acknowledgements**

Nur Thaqifah Salihah would like to thank the Ministry of Education, Brunei Darussalam for the opportunity to undertake a Ph.D programme at Universiti Brunei Darussalam (UBD).

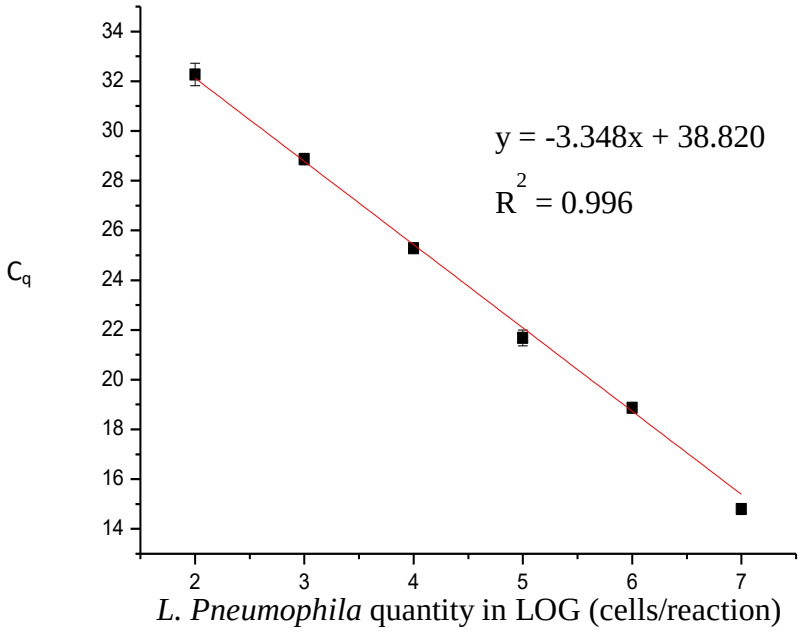


***Figure 3.*** Standard amplification curve for ZEN™ probe P1mip for *L. pneumophila* ATCC 33152 DNA with dilutions between $1\times10^2$ and $1 \times 10^7$ cell/reactions. $C_q$ (the quantification cycle) indicates the number of PCR cycles needed to produce adequate amounts of PCR products to yield a fluorescent signal strong enough to cross the threshold limit for a signal detectable above noise.[5]

***Table 5.*** Ratio of positive reaction and inter- and intra-assay coefficient variation (CV%) for the P1mip real-time PCR assays within the range of $1 \times10^3$ to $1\times10^7$ cells of *S. aureus* DNA dilution ZEN™ double-quenched probes.

| Assay | cell/reaction | Ratio of positive reactions[a] | Mean CV% ± SD[b] | |
|---|---|---|---|---|
| | | | Intra-assay | Inter-assay |
| P1mip | $1 \times 10^7$ | 9/9 | 0.749 ± 0.082 | 0.699 ±0.349 |
| | $1 \times 10^6$ | 9/9 | | |
| | $1 \times 10^5$ | 9/9 | | |
| | $1 \times 10^4$ | 9/9 | | |
| | $1 \times 10^3$ | 9/9 | | |
| | $1 \times 10^2$ | 6/9 | | |

[a] number of positive result per 9 individual reactions

[b] SD is standard deviations

**References**


[1] H. Friedman, Y. Yamamoto and T.W. Klein, *Semin Pediatr Infect Dis*., **2002**, 13, 273-279.

[2] J.E. McDade, C.C. Shepard, D.W. Fraser, T.R. Tsai, M.A. Redus and W.R. Dowdle, *N Engl J Med.*, **1977**, 297, 1197-1203.

[3] D.W. Fraser, T.R. Tsai, W. Orenstein, W.E. Parkin, H.J. Beecham, R.G. Sharrar, J. Harris, G.F. Mallison, S.M. Martin, J.E. McDade, C.C. Shepard, , P.S. Brachman, *N. Engl. J. Med*., **1977**, 297, 1189– 1197.

[4] A.W. Ensminger, *Curr Opin Microbiol.*, **2016**, 29, 74-78.

[5] N.T. Salihah, M.M. Hossain, H. Lubis, M.U. Ahmed, *J Food Sci Technol.*, **2016**, 53, 2196-2209.

[6] N. Wellinghausen, C. Frost, R. Marre, *Appl Environ Microbiol.*, **2001**, 67, 3985-3993.

[7] K.E. Templeton, S.A. Scheltinga, P. Sillekens, J.W. Crielaard, A.P. van Dam, H. Goossens and E.C.J. Claas, *J Clin Microbiol.*, **2003**, 41, 4016-4021.

[8] M.A. Yáñez, C. Carrasco-Serrano, V.M. Barberá, V. Catalán, *Appl. Environ. Microbiol.*, **2005**, 71, 3433-3441.

[9] W. Ahmed, H. Brandes, P. Gyawali, J.P.S. Sidhu, S. Toze, *Water Res.*, **2014**, 53, 361-369.

[10] D.A. Wilson, B. Yen-Lieberman, U. Reischl, S.M. Gordon and G.W. Procop, *J Clin Microbiol.*, **2003**, 41, 3327-3330.

[11] N.C. Engleberg, C. Carter, D.R. Weber, N.P. Cianciotto and B.I. Eisenstein, *Infect Immun.*, **1989**, 57, 1263-1270.

[12] https://www.ncbi.nlm.nih.gov/genbank/

[13] https://www.ncbi.nlm.nih.gov/tools/primer-blast/

[14] J. Guo, X. Yang, Z. Cen, R. Yang, Y. Cui and Y. Song, NCBI GenBank, **2014**. https://www.ncbi.nlm.nih.gov/nuccore/NZ_JFIP00000000.1 [Accessed 6 May 2017].

[15] S. Ditommaso, M. Gentile, M. Giacomuzzi and C.M. Zotti, *Diagn Microbiol Infect Dis.*, **2011**, 70, 200-206.

[16] J. Behets, P. Declerck, Y. Delaedt, B. Creemers and F. Ollevier, *J Microbiol Methods.*, **2007**, 68, 137-144.

[17] J.F. Martínez-Blanch, G. Sánchez, E. Garay, R. Aznar, *Int J Food Microbiol*. **2009,** 135, 15-21.

[18] D. Klein, P. Janda, R. Steinborn, M. Müller, B. Saimons and W.H. Günzburg, *Electrophoresis*, **1999**, 20, 291-299.

[19] G. Johnson, T. Nolan and S.A. Bustin, *Methods Mol Biol.*, **2013,** 943, 1–16.

[20] V. Fusco, G.M. Quero, M. Morea, G. Blaiotta, A., *Int J Food Microbiol*, **2011**, 144, 528-537.

# Adsorption of brilliant green dye on *Nephelium mutabile* (Pulasan) leaves

*Nur Afiqah Hazirah Mohamad Zaidi[1*], Liew Wei Jing[1] and Linda B. L. Lim[1]*

*[1]Department of Chemical Sciences, Faculty of Science, Universiti Brunei Darussalam, Jalan Tungku Link, Gadong, BE1410, Brunei Darussalam*

**corresponding author email: afhazirah@gmail.com*

**Abstract**

The main objective of this study is to investigate the ability of *Nephelium mutabile* (Pulasan) leaves (PL) in removing toxic brilliant green (BG) dye using the adsorption method. Batch experiments were conducted on the adsorption of BG dye using PL with a contact time of 3.5 h. Adsorption isotherm studies were analysed using six isotherm models, namely Langmuir, Freundlich, Temkin, Dubinin-Radushkevich (D-R), Redlich-Peterson (R-P) and Sips, and the results showed that Sips is the model that best fits the experimental data, with a maximum adsorption capacity ($a_{max}$) of 130.3 mg $g^{-1}$. The point of zero charge ($pH_{PZC}$) of PL was found to be at pH 5.29. Regeneration studies showed that PL can be recovered and reused, especially after treatment with NaOH. This study demonstrates that PL can be considered as a reasonably good and cost-effective biosorbent for BG under our experimental conditions.

*Index Terms: Nephelium mutabile*, adsorbent, adsorption isotherm, brilliant green dye

## 1. Introduction

Dye is generally used to colour substances, either by soaking the material in a solution impregnated with a dye or directly on the fiber. In the latter case, a mordant is required in order to improve the fastness of the dyeing process.[1] Dyes can be from natural or synthetic sources. Both dyes and pigments are coloured because they absorb only some wavelengths of visible light. Dyes are usually soluble in water whereas pigments are insoluble. Some dyes can be rendered insoluble with the addition of salt to produce a lake pigment.[2] The majority of natural dyes are derived from plant sources: roots, berries, bark, leaves, and wood, fungi, and lichens.[3] However, the discovery of man-made synthetic dyes in the late 19th century ended the large-scale market for natural dyes.[4] Synthetic dyes are made from petroleum, sometimes in combination with mineral-derived components.[1] Many dyes are organic compounds.[5] The dyes are classified according to their solubility and chemical properties. There are different types of dyes: acidic, basic, mordant, reactive and dispersive dyes.[6] These dyes are produced and applied in large quantities by many different industries. Therefore, it is a challenge to treat dye effluents because of their synthetic origins and complex aromatic structures, which are biologically non-degradable and could be harmful to health.

*Nephelium mutablie*, often called Pulasan or wild rambutan, belongs to the family Sapindaceae, which is a tropical seasonal fruit closely allied to the *Nephelium lappaceum* (rambutan). The fruits are quite popular as it is sweeter than the rambutan and lychee, but it is very rare outside Southeast Asia. Pulasan is a seasonal fruit and, during the period of this study, the Pulasan fruits were not in season. So instead of using the fruit peel, Pulasan leaves (PL) were chosen as the adsorbent. Furthermore, the leaves are in abundance throughout the year, a necessary criterion for a low-cost adsorbent. Because of this, this project utilized PL in the adsorption of a selected dye, *viz.* brilliant green (BG) dye.

BG is one of the triarylmethane dyes with the chemical formula $C_{27}H_{33}N_2.HO_4S$ and a molecular weight of 482.64 g $mol^{-1}$. When

dissolved in water, it gives a blue-coloured solution with a maximum absorbance at a wavelength of 624 nm. BG is used widely in many industries to colour silk and wool. Even the dilute alcoholic solution of BG is sold in Eastern Europe and Russia as a topical antiseptic due to its effectiveness against Gram-positive bacteria.[7,8] The main advantage of BG over more common antiseptics such as iodine is that it does not irritate mucous membranes as harshly. However, if swallowed, BG can induce vomiting and it can be toxic upon ingestion. If BG comes in contact with the eyes, it can cause corneal opacification and lead to bilateral blindness.[9] Hence, the potential of PL as a low-cost adsorbent in the removal of BG from aqueous solutions is worth investigating.

## 2. Experimental approach

*2.1 Sample preparation and chemical reagents*

The Pulasan leaves (PL) were freshly plucked from a tree and washed with water for several times to remove dust on the surface. Then they were thoroughly rinsed with distilled water and dried in an oven at 80$^{o}$C for about a week, to remove all moisture, until a constant mass was obtained. The dried sample was blended using a blender and sieved using a laboratory metal sieve to obtain a particle size of less than 355 µm. The sieved sample was stored in a zip-lock plastic bag to prevent moisture build-up and avoid contamination.

Brilliant green (BG) dye with a percentage purity of 90% was purchased from Sigma Aldrich Corporation, and was used without further purification. 1000 mg $L^{-1}$ of BG stock solution was prepared by dissolving 1 g of the dye in distilled water in a 1 L volumetric flask. To obtain solutions of different concentrations, this stock solution was appropriately diluted by adding distilled water.

*2.2 Calibration curve*

For the calibration curves of the BG dye, 2, 4, 6, 8 and 10 mg $L^{-1}$ concentrations of standard solutions were prepared.

*2.3 Instrumentation*

To measure the absorbance of the BG solutions, a Shimadzu UV-1601PC spectrophotometer was used at a wavelength of 624 nm. Also, a Stuart Scientific Flask Shaker $SF_1$ was used to mix the adsorbent with the dye solution at 250 rpm. In order to identify the functional groups present in the PL, a Shimadzu IRPrestige-21 spectrophotometer (FTIR) Scanning Electron Microscope (SEM) was used to observe the morphology of the adsorbent's surface.

*2.4 Adsorption studies*

Similar procedures as reported by Lim *et al.*[10] were followed in this study to investigate the effects of contact time, pH, and ionic strength on the adsorption of BG onto the PL. However, there were slight changes to the methods cited above, as the concentration of BG used to test the effects of contact time was 100 mg $L^{-1}$ and an additional three salts were used to test the effects of ionic strength, namely NaCl, $NaNO_3$ and KCl, as well as $KNO_3$.

For regeneration studies of the spent adsorbent, 0.4 g of the adsorbent was placed into a 500 mL conical flask containing 200.0 mL of 100 mg $L^{-1}$ dye solution. The ratio of the volume of dye to the mass of adsorbent was 1:500, as 1 g of sample was mixed with 500.0 mL of dye. The flask was then shaken using a shaker at 250 rpm at room temperature for an optimum shaking time. After filtration, the solid residues were collected and dried in an oven at around 60 ℃ overnight, while the filtrate was diluted to 10 mg $L^{-1}$ for the analysis of absorbance using the UV-Vis spectrophotometer.

The dried solid residues were weighed and divided into five portions in 250 mL labelled conical flasks for treatment purposes. The residual solids were treated with HCl (0.1 M), NaOH (0.1 M), distilled water (shake and rinse) and a control was also set up. In the treatments with acid, base and distilled water, the volumes used were chosen to give a 1:20 ratio. After being washed with desorbing agents, the residues were placed back in the oven to dry. This alternation of

adsorption and desorption steps was continued for five consecutive cycles.

### 3. Characterization of PL

The point of zero charge ($pH_{PZC}$) was used to determine the pH at which the adsorbent's surface has zero charge. ***Figure 1*** shows that the $pH_{PZC}$ of the PL was determined to be pH 5.29. This value can be determined from the point of intersection of the plot of ΔpH against the initial pH at which the ΔpH is zero (see ***Figure 1***). When the pH is less than $pH_{PZC}$, the adsorbent's surface will be predominantly positively charged due to protonation and hence will attract anions from the solution. By contrast, at pHs greater than the $pH_{PZC}$, the adsorbent's surface will be predominantly negatively charged due to deprotonation and hence attract cations from the solution. In this case, when pH < 5.29 the PL's surface is expected to be positively charged, and negatively charged when pH > 5.29. At pH = 5.29 the PL's surface has zero net charge.

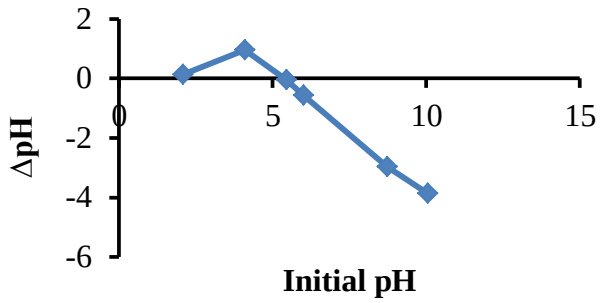


***Figure 1.*** Plot to determine the point of zero charge of PL. (Mass of adsorbent: 0.05 g; volume of $KNO_3$: 25.0 mL; conc. of $KNO_3$: 0.1 mol $L^{-1}$; room temperature; pH: 2-10)

The SEM images of the PL, before and after adsorption with BG, are shown in ***Figure 2*** with a magnification of 800x. Untreated PL, as shown in ***Figure 2 (a)***, have a rough, undulating surface with many folds. However, after adsorption of BG, there was a distinct change in the surface morphology of the PL, indicating that BG was adsorbed, as shown in ***Figure 2 (b).***

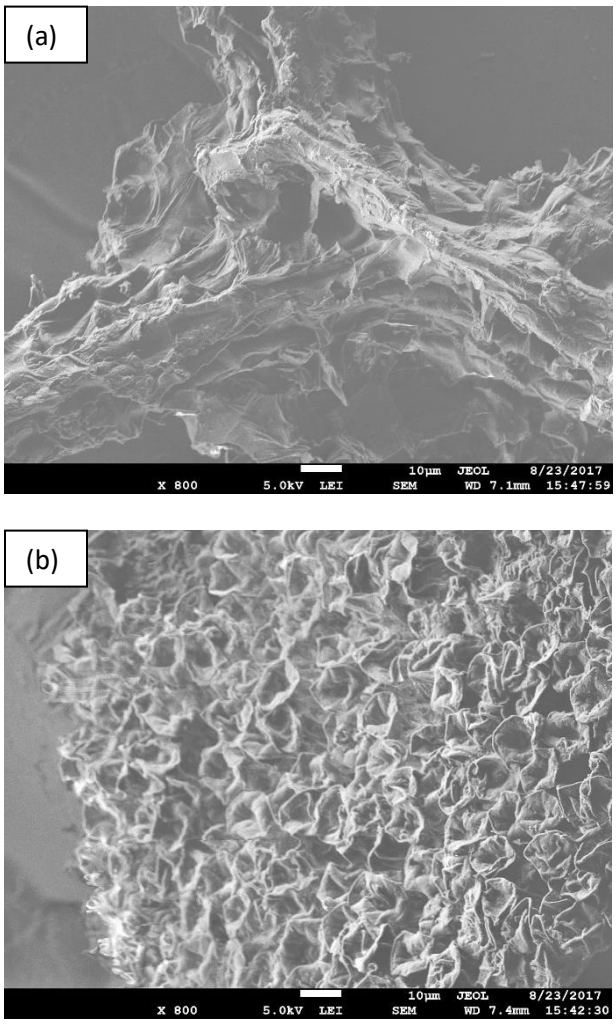


***Figure 2.*** SEM images of the PL (a) untreated and (b) treated with BG at 800x magnification

***Figure 3*** shows the FTIR spectra of the untreated PL and the BG-loaded PL. As can be observed from the spectrum of the untreated PL (in black), functional groups such as alkenes (C=C) at 1621 $cm^{-1}$, C=O at about 1724 $cm^{-1}$, alkyls (CH) at 2926 $cm^{-1}$, and amines (NH) and hydroxyls (OH) at 3309 $cm^{-1}$ are present. After being treated with BG, the spectrum (in blue) indicated shifts in the amino, hydroxyl, alkene and carboxyl groups, which suggests that these groups could be involved in the adsorption of BG dye.

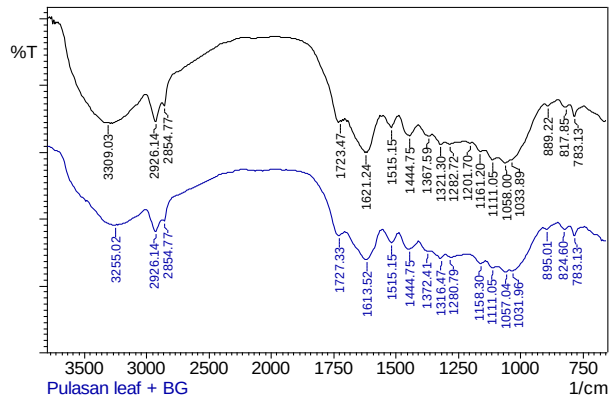


***Figure 3.*** FTIR spectra of the untreated PL (black) and the PL treated with BG (blue)

## 4. Results and Discussion.

*4.1 Effect of contact time*

***Figure 4*** shows the extent of the adsorption of BG by the PL adsorbent over four hours. Approximately 65% of the BG dye was adsorbed by the PL and equilibrium was reached within 210 minutes. It can be observed that there was a rapid adsorption of BG dye for the first 30 minutes of the contact time. This was due to the availability of vacant sites on the surface of the adsorbent, together with the high concentration of the dye. After some time, the rate of adsorption slowed down until it reached equilibrium, once all the sites on the adsorbent were occupied by dye molecules. Hence the contact time used for the rest of the study was set at 3.5 hours to ensure that complete equilibrium was reached.

*4.2 Effects of pH*

In real-life situations, the actual pH of the wastewater may be more acidic or basic than the ambient pH, thus there is a need to study the effects of pH.[11] Investigation of the effects of the pH of the dye solution on the adsorption capacity of PL should consider possible changes in both the degree of ionization of the dye and its surface properties.[12] As a result of these changes, the ability of an adsorbent to adsorb dye will vary with the pH of the aqueous solution. A study of the adsorption process was therefore performed using different pHs of BG, and the results are shown in ***Figure 5***.

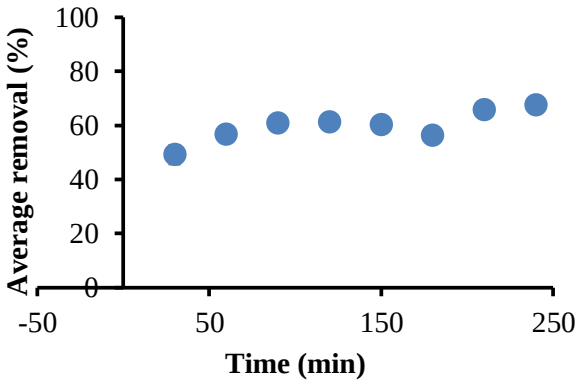


***Figure 4.*** Effect of contact time on the removal of BG (Mass of adsorbent: 0.050 g; volume of BG: 25.0 mL; conc. of BG: 100 mg $L^{-1}$; room temperature; ambient pH)

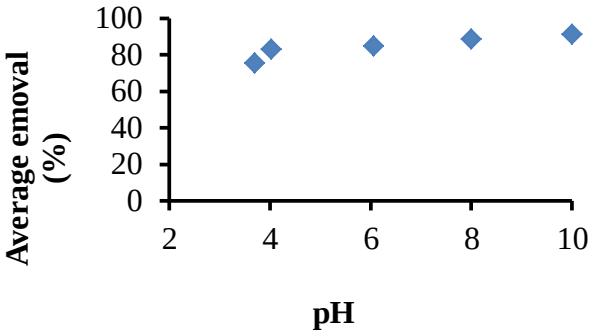


***Figure 5.*** The effect of pH on the adsorption of BG onto the PL (Mass of adsorbent: 0.050 g; volume of BG: 25.0 mL; conc. of BG: 100 mg $L^{-1}$; room temperature; pH: ambient (3.69), 4.02, 6.06, 8 and 10)

A previous report by Chieng *et al.*[13] has shown that BG is unstable at extreme pHs. Hence, this study was limited to pHs between 3.7 and 10. The recorded untreated (ambient) pH of BG was 3.69, and at this pH removal of about 75% of BG dye was observed. Above this pH, from pH 4.02 to 10.0, there was a slight increase in the removal of BG dye which was probably due to a decrease in the concentration of $H^+$ ions in the aqueous solution and also due to the electrostatic attraction between the adsorbent and the dye molecules. This study shows that the PL has the ability to adsorb BG over a wide range of pHs. Unlike adsorbents such as *Luffa cylindrica* sponge[14] and some reported agriculture wastes,[15] which show a decrease in adsorption of BG at

higher pHs, PL are resilient to changes in the pH of the medium. This is an advantage especially in real-life applications of wastewater treatment, where the pH varies.

*4.3 Adsorption isotherm of BG onto the PL*

Batch adsorption isotherm was carried out at room temperature using BG concentrations ranging from 0 to 1000 mg $L^{-1}$. The experimental data obtained were fitted to six different isotherm models, namely Langmuir,[16] Freundlich,[17] Temkin,[18] Dubinin-Radushkevich (D-R),[19] Redlich-Peterson (R-P)[20] and Sips,[21] the linear equations for which are shown in ***Table 1***. Six error functions (shown in ***Table 2***) were used to help in identifying the best-fit model, especially in situations where all the models were in close agreement with the experimental data.

***Table 1.*** Brief descriptions of the types of isotherm used.[16-21] [Here, $C_e$ is the equilibrium concentration of dye solution (mg $L^{-1}$); $q_e$ is the equilibrium dye concentration on the bio-sorbent (mmol $g^{-1}$); $q_{max}$ is the maximum adsorption capacity of the PL for BG; $K_L$, $K_F$, $K_T$, $K_R$ and $K_S$ are the Langmuir, Freundlich, Temkin, Redlich-Peterson and Sips adsorption constants respectively; $n$ (in the Freundlich model) is an empirical parameter related to the adsorption capacity and is typically in the range $0 < n < 1$; $b_T$ is the Temkin constant related to the heat of adsorption; $R$ is the gas constant; and $T$ is the temperature (in Kelvin) at which the adsorption takes place.]

| Isotherm Model | Linearized Equation | Linear Plots |
|---|---|---|
| Langmuir | $\frac{C_e}{q_e} = \frac{1}{q_{max}} C_e + \frac{1}{q_{max}}\left(\frac{1}{K_L}\right)$ | $\frac{C_e}{q_e} vs. C_e$ |
| Freundlich | $\log q_e = \frac{1}{n}\log C_e + \log K_F$ | $\log q_e vs. \log C_e$ |
| Temkin | $q_e = \left(\frac{RT}{b_T}\right)\ln K_T + \left(\frac{RT}{b_T}\right)\ln C_e$ | $q_e vs. \ln C_e$ |
| Dubinin-Radushkevich (D-R) | $\ln q_e = \ln q_{max} - \beta\varepsilon^2$<br>where β is the D-R constant,<br>Polanyi potential: $\varepsilon = RT\ln\left(1+\frac{1}{C_e}\right)$<br>Mean free energy: $E = \frac{1}{\sqrt{2\beta}}$ | $\ln q_e\ vs.\ \beta\varepsilon^2$ |
| Redlich-Peterson (R-P) | $\ln\left(\frac{K_R C_e}{q_e} - 1\right) = n\ln C_e + \ln a_R$ | $\ln\left(\frac{K_R C_e}{q_e} - 1\right) vs. \ln C_e$ |
| Sips | $\ln\left(\frac{q_e}{q_{max} - q_e}\right) = \frac{1}{n}\ln C_e + \ln K_S$ | $\ln\left(\frac{q_e}{q_{max} - q_e}\right) vs. \ln C_e$ |

***Figure 6*** shows simulated plots of the six chosen isotherm models together with the experimental data. The linear regression coefficients ($R^2$) and error values of the six isotherm models used are shown in ***Table 3***. Based on the simulation plots, it is clear that the D-R model deviates from the experiment data and hence can be ruled out. All the other five models are in good agreement with the experimental data. Even though the Sips model does not give the highest $R^2$ value, it was chosen as the best isotherm model since it has the lowest overall error values when compared to the other models, and its $R^2$ value is good (> 0.95). The Langmuir model, which describes monolayer adsorption, gives the highest $R^2$ value, but its overall errors are much higher.

The maximum adsorption capacity ($q_{max}$) of the PL based on the Sips and Langmuir models is 130.3 mg $g^{-1}$ and 102.6 mg $g^{-1}$, respectively, as shown in ***Table 3***. In comparison with the other selected adsorbents (see ***Table 4***), PL have a higher $q_{max}$ than some natural adsorbents (e.g. Luffa sponge, kaolin) and even adsorbents that have undergone modification with an acid (almond peel) or a base (saw dust). However, their $q_{max}$ is lower than some reported adsorbents such as peels of pomelo and *Artocarpus odoratissimus.* Nevertheless, PL have a good $q_{max}$, making it a potentially useful adsorbent for real-life wastewater treatment.

*4.4 Effects of ionic strength*

In a real-life situations, the wastewater produced by industrial processes may be polluted with different kinds of cations and anions with different concentrations.[11] In this study, the effects of ionic strength were investigated to see if increasing the concentrations of NaCl, $NaNO_3$, KCl or $KNO_3$ (0, 0.01, 0.1, 0.2, 0.4, 0.6, 0.8 and, 1.0 mg $L^{-1}$) influences the adsorption of 100 mg $L^{-1}$ of BG on the PL.

***Figure 7*** shows the effects of varying ionic strengths on the adsorption of BG dye. It can be observed that as the concentration of all the salts increases from 0 to 1.0 mg $L^{-1}$, the percentage removal of the BG dye decreases. Initially, the presence of the salts tends to affect the interactions between the PL and BG through competition between the cations from the salts ($Na^+$ and $K^+$) with the cationic BG for the available active sites on the PL.[30-31] The increase in the salt concentrations also indirectly disturbs the equilibrium, which can affect the operation of the adsorption of BG onto the PL.[32]

***Table 2.*** The six error functions used. [Here, $q_{e,meas}$ and $q_{e,calc}$ are the experimental and calculated values respectively; $n$ is the number of experimental data points and $p$ is the number of parameters in the model.]

| **Type of errors** | **Equations** |
|---|---|
| Average relative error (ARE) | $\frac{100}{n}\sum_{i=1}^{n}\left\lvert\frac{q_{e,meas}-q_{e,calc}}{q_{e,meas}}\right\rvert_i$ |
| Sum square error (SSE) | $\sum_{i=1}^{n}(q_{e,calc}-q_{e,meas})_i^2$ |
| Hybrid fractional error function (HYBRID) | $\frac{100}{n-p}\sum_{i=1}^{n}\left[\frac{(q_{e,meas}-q_{e,calc})^2}{q_{e,meas}}\right]_i$ |
| Sum of Absoulte Error (EABS) | $\sum_{i=1}^{n}\lvert q_{e,meas}-q_{e,calc}\rvert$ |
| Marquardt's percent standard deviation (MPSD) | $100\sqrt{\frac{1}{n-p}\sum_{i=1}^{n}\left(\frac{q_{e,meas}-q_{e,calc}}{q_{e,meas}}\right)_i^2}$ |
| Non-linear Chi-Square ($\varkappa^2$) | $\sum_{i=1}^{n}\frac{(q_{e,meas}-q_{e,calc})^2}{q_{e,meas}}$ |

***4.5 Regeneration studies***

A regeneration study of the adsorbent is important because it helps in the recovery of the adsorbates, especially where precious metals are involved, and the reusability of adsorbents reduces the costs of wastewater treatment. In this study, three solvents (HCl, NaOH and distilled water) were used to treat the BG-loaded adsorbent, and the study was carried out for five consecutive cycles. A control experiment was also carried out for comparison purposes.

The spent PL adsorbent can be reused while retaining similar adsorption capabilities even in the fifth cycle, as shown by the control experiment shown in ***Figure 8***. Furthermore, successive treatment of the PL with HCl, NaOH or distilled water all showed that the spent PL

were still able to remove BG well, even after the fifth cycle. Both acid and base treatments were able to enhance the adsorption capacity of the PL, with NaOH being the most effective method of regeneration.

## 5. Conclusion.

In conclusion, PL have the potential to be used as a low-cost adsorbent for the removal of BG, as they have a high maximum adsorption capacity for the removal of BG. The adsorption of BG is best described by the Sips isotherm model. The presence of high concentrations of salts in the aqueous solution seems to have a great influence on the adsorption of BG. Nonetheless, the ability to regenerate and be reused further enhances the potential of the PL as a possible adsorbent for removing BG.

***Table 3.*** The adsorption isotherm constants, linear regression coefficient ($R^2$) and error functions for the six isotherm models used to describe the adsorption of BG onto the PL.

| Model | | | Error functions | | | | | |
|---|---|---|---|---|---|---|---|---|
| | | $R^2$ | ARE | SSE | HYBRID | EABS | MPSD | $\varkappa^2$ |
| **Langmuir** | | 0.9833 | 16.71 | 0.0041 | 0.32 | 0.23 | 22.21 | 0.049 |
| $q_{max}$ (mmol $g^{-1}$) | 0.21 | | | | | | | |
| $q_{max}$ (mg $g^{-1}$) | 102.63 | | | | | | | |
| $K_L$ (L $mmol^{-1}$) | 0.03 | | | | | | | |
| **Freundlich** | | 0.9366 | 16.73 | 0.0034 | 0.36 | 0.17 | 31.88 | 0.055 |
| $K_F$ (mmol $g^{-1}$) | 0.03 | | | | | | | |
| $K_F$ ($mg^{1-1/n}$ $L^{1/n}$ $g^{-1}$) | 13.13 | | | | | | | |
| n | 2.97 | | | | | | | |
| **Temkin** | | 0.9603 | 13.87 | 0.0029 | 0.25 | 0.17 | 21.28 | 0.037 |
| $K_T$ (L $mmol^{-1}$) | 0.47 | | | | | | | |
| $b_T$ (kJ $mol^{-1}$) | 66.45 | | | | | | | |
| **Dubinin-Radushkevish** | | 0.8895 | 115.25 | 0.084 | 12.56 | 0.99 | 187.52 | 1.89 |
| $q_{max}$ (mmol $g^{-1}$) | 0.16 | | | | | | | |
| $q_{max}$ (mg $g^{-1}$) | 76.87 | | | | | | | |
| B (J $mol^{-1}$) | $7.29x10^{-7}$ | | | | | | | |
| E (kJ $mol^{-1}$) | 827.94 | | | | | | | |
| **Redlich Peterson** | | 0.9821 | 15.94 | 0.0031 | 0.35 | 0.17 | 30.45 | 0.048 |
| $K_R$ (L $g^{-1}$) | 0.05 | | | | | | | |
| $\alpha$ | 0.70 | | | | | | | |
| $a_R$ (L $mmol^{-1}$) | 1.48 | | | | | | | |
| **Sips** | | 0.9518 | 14.52 | 0.0029 | 0.24 | 0.18 | 20.10 | 0.034 |
| $q_{max}$ (mmol $g^{-1}$) | 0.27 | | | | | | | |
| $q_{max}$ (mg $g^{-1}$) | 130.32 | | | | | | | |
| $K_S$ (L $mmol^{-1}$) | 0.05 | | | | | | | |
| n | 1.45 | | | | | | | |

## Acknowledgements

The authors are grateful to the Government of Negara Brunei Darussalam and Universiti Brunei Darussalam (UBD) for their support, as well as to the Physical and Geological Sciences Group at UBD for the use of their SEM instrument.

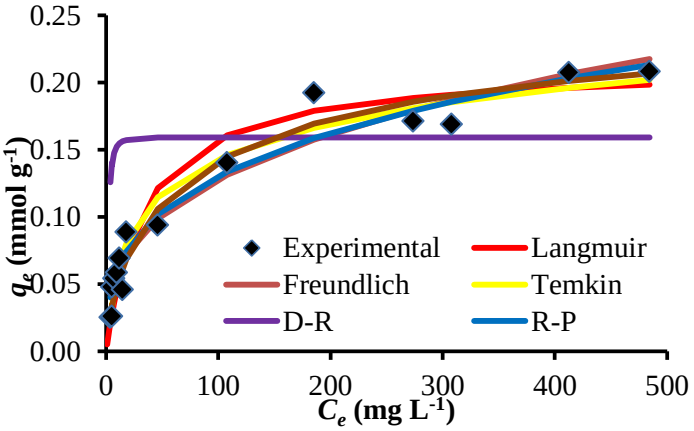


***Figure 6.*** Simulation plots of the six isotherm models, together with the experimental data for the adsorption of BG onto the PL (Mass of adsorbent: 0.050 g; volume of BG: 25.0 mL; conc. of BG: 0-1000 mg $L^{-1}$; room temperature; ambient pH)

**Table 4.** Maximum adsorption capacity ($q_{max}$) of the PL and other reported adsorbents for the removal of BG.

| **Adsorbent** | **$q_{max}$ (mg $g^{-1}$)** | **Reference** |
|---|---|---|
| *Nephelium mutabile* (pulasan) leaves | 130.3 (Sips)<br>102.6 (Langmuir) | This study |
| Peat | 265.0 | [13] |
| *Luffa cylindrica* sponge | 18.2 | [14] |
| Acid treated almond peel | 30.0 | [22] |
| NaOH treated saw dust | 58.5 | [23] |
| Kaolin | 65.4 | [24] |
| Red clay | 125.0 | [25] |
| Pomelo skin | 325.0 | [26] |
| Rice straw biochar | 111.1 | [27] |
| *Artocarpus odoratissimus* peel | 174.0 | [28] |
| Cempedak durian peel | 98.0 | [29] |

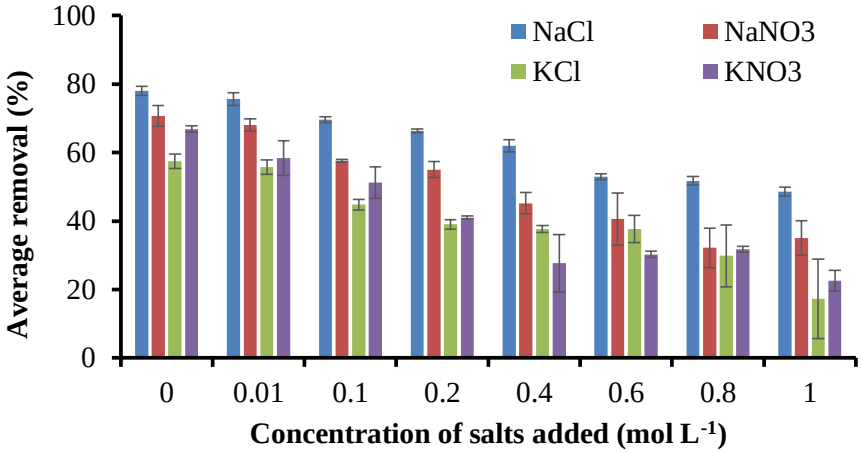


***Figure 7.*** The effect of ionic strength on the adsorption of BG using four salts (Mass of adsorbent: 0.05 g; volume of BG: 25 mL; conc. of BG: 100 mg $L^{-1}$; room temperature; pH: ambient; types of salt: KCl, NaCl, $KNO_3$, $NaNO_3$; conc. of salt: 0 to 1 mol $L^{-1}$)

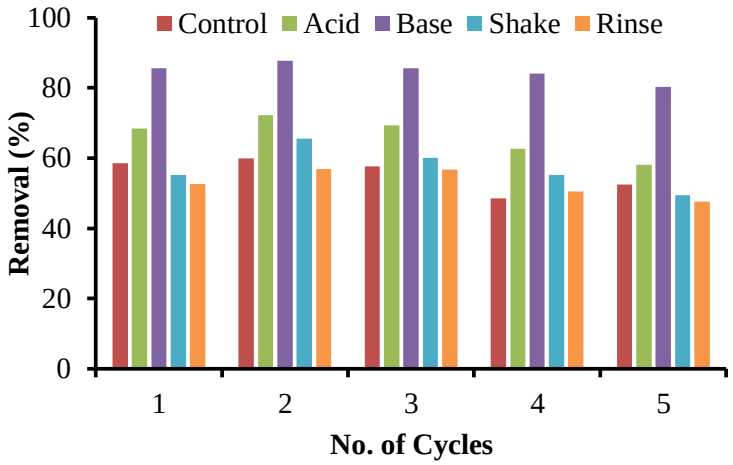


***Figure 8.*** Regeneration of PL for five consecutive cycles with different desorbing agents (Ratio of mass of adsorbent and volume of BG: 1 g: 500 mL; conc. of BG: 100 mg $L^{-1}$; room temperature, pH: ambient; desorbing agents: HCl, NaOH, water; ratio of mass of adsorbent and volume of desorbing agents: 1 g: 50 mL; conc. of HCl and NaOH: 0.1 mol $L^{-1}$)

## References


[1] S. Purwar, *Int. J. Home Sci*., **2016**, 2, l283-287.

[2] C. Anselmi, D. Capitani, A. Tintaru, B. Doherty, A. Sgamellotti and C. Miliani, *Dyes Pigm*., **2017**, 140, 297-311.

[3] K. G. Gilbert and D. T. Cooke, *Plant Growth Regul.* **2001**, 34, 57-69.

[4] H. V. Belt and A. Rip, Cambridge, MA: MIT Press, **1987**, 135-158.

[5] M. T. Yagub, T. K. Sen, S. Afroze and H. M. Ang, *Adv. Coll. Interf. Sci*., **2014**, 209, 172-184.

[6] K. M. Abuamer, A. A. Maihub, M. M. El-Ajaily, A. M. Etorki, M. M. Abou-Krisha and A. Almagani, *Int. J. Org. Chem*., **2014**, 4, 7-15.

[7] S. M. Susarla, J. B. Mulliken, L. B. Kaban, P. N. Manson and T. B. Dodson, *Int. J. Oral Maxillofac. Surg*., **2017**, 46, 401-403.

[8] S. Hashemian, A. Dehghanpor and M. Moghahed, *J. Indust. Eng. Chem*., **2015**, 24, 308-314.

[9] B. H. Shambharkar and A. P. Chowdhury, *RSC Adv*., **2016**, 6, 10513-10519.

[10] L. B. L. Lim, N. Priyantha and N. A. H. M. Zaidi, *Environ. Earth Sci*., **2016**, 75, 1179.

[11] L. B. L. Lim, N. Priyantha, M. H. F. Lai, R. M. Salleha and T. Zehra, *Int. Food. Res. J*., **2015**, 22(3), 1043-1052

[12] N. J. Ara, M. A. Rahman and A. S. M. Alam, *Bangladesh J. Sci. Indust. Res.*, **2015**, 50, 285-292.

[13] H. I. Chieng, N. Priyantha and L. B. L. Lim, *RSC Adv.*, **2015**, 5, 34603-34615.

[14] O. S. Esan, O. N. Abiola, O. Owoyomi, C. O. Aboluwoye and M. O. Osundiya, *ISRN Phys. Chem.*, **2014**, 14, Article ID 743532

[15] A. Karuppasamy, P. Muthirulan and M. M. Sundaram, *J. Chem. Pharm. Res*., **2012**, 4, 5101-5110.

[16] I. Langmuir, *J. Am. Chem. Soc.*, **1916**, 38, 2221-2295.

[17] H. M. F. Freundlich, *J. Phys. Chem.*, **1906**, 57, 385-470.

[18] M. I. Temkin and V. Pyzhev, *Acta Physiochimica USSR.*, **1940**, 12, 327-356.

[19] M. M. Dubinin and L. V. Radushkevich, *Proc. Acad. Sci.*, **1947**, 55, 327.

[20] O. Redlich and D. L. Peterson, *J. Phys. Chem.*, **1959**, 63:1024-1029.

[21] R. Sips, *J. Chem. Phy.*, **1948**, 16, 490-495.

[22] R. Ahmad and P. K. Mondal, *Sep. Sci. Technol.*, **2009**, 44, 1638-1655.

[23] V. S. Mane and P. V. V. Babu, *Desalin*., **2011**, 273, 321-329.

[24] B. K. Nandi, A. Goswami and M. K. Purkait, *J. Hazard. Mater*., **2009**, 161, 387-395.

[25] M. S. U. Rehman, M. Munir, M. Ashfaq, N. Rashid, M. F. Nazar, M. Danish and J. -I. Han, *Chem. Eng. J.*, **2013**, 228, 54-62.
[26] M. K. Dahri, M. R. R. Kooh and L. B. L. Lim, *Scientia Bruneiana*, **2017**, 16, 49-56.
[27] M. S. U. Rehman, I. Kim, N. Rashid, M. Adeel Umer, M. Sajid and J. I. Han, *CLEAN Soil Air Water*, **2016**, 44, 55-62.
[28] M. K. Dahri, L. B. L. Lim, M. R. R. Kooh and C. M. Chan, *Int. J. Environ. Sci. Technol*., **2017**, 14, 2683-2694.
[29] M. K. Dahri, L. B. L. Lim and C.C. Mei, *Environ. Monit. Assess*., **2015**, 187, 546.
[30] S. Afroze, T. K. Sen, M. Ang and H. Nishioka, *Desalin. Water Treat.*, **2016**, 57, 5858-5878.
[31] W. -H. Li, Q. -Y. Yue, B. -Y. Gao, Z .-H. Ma, Y. -J. Li and H. -X. Zhao, *Chem. Eng. J*., **2011**, 171, 320-327.
[32] S. Dawood, T. K. Sen and C. Phan, *Desalin. Water Treat*., **2016**, 57, 28964-28980.

# Linking Geostatistical Methods: Co-Kriging – Principal Component Analysis (PCA); with Integrated Well Data and Seismic Cross Sections for Improved Hydrocarbon Prospecting (Case Study: Field X)

*Ryan Bobby Andika[1*] and Haritsari Dewi[1]*

*[1]Department of Geophysical Engineering, Faculty of Mining and Petroleum Engineering, Institut Teknologi Bandung, Jalan Ganeca 10, Bandung 40132, Indonesia*

**corresponding author email: ryanbobbyandikaandika@yahoo.com*

**Abstract**

In this era of globalization, the demand for energy is rising in tandem with social and economic development throughout the world. Current hydrocarbon demand is much greater than domestic crude oil and natural gas production. In order to bridge the gap between energy supply and demand, it is imperative to accelerate exploration activities and develop new effective and efficient techniques for discovering hydrocarbons. Therefore, this study presents a new method for integrating seismic inversion data and well data using geostatistical principles that allow for the high level of processing and interpretation expected nowadays. The main part of this paper will concern the preparation and processing of the input data, with the aim of constructing a map of hydrocarbon-potency distribution in a certain horizon. It will make use of principal component analysis (PCA) and the co-kriging method. In the case study of Field X, we analyze a single new dataset by applying PCA to every existing well that contains multivariate rock-physics data. The interpretation that can be extracted from the output gives us information about the hydrocarbon presence in a particular depth range. We use that output as our primary dataset from which our research map is constructed by applying the co-kriging method. We also rely on an acoustic impedance dataset that is available for a certain horizon to fulfill the co-kriging interpolation requirement. All of the acoustic impedance data and output data that result from the application of PCA in a particular horizon give strong correlation factors. Our resulting final map is also validated with information from proven hydrocarbon discoveries. It is demonstrated that the map gives accurate information suggesting the location of hydrocarbon potency, which will need some detailed follow-up work to enhance the distribution probabilities. This method can be considered for hydrocarbon prediction in any area of sparse well control.

*Index Terms:* co-kriging, PCA, spatial relations, well data, AI seismic inversion

## 1. Introduction

In earth sciences, we seldom have sufficient data to accurately reveal the entire underlying subsurface conditions. Typically, in prospecting hydrocarbon zonation, we have to estimate the input parameters for the entire area from only a few data points. The existence of log data from the wells facilitates the descriptions of the petrophysical rock parameters. The more well data, the more accurate the geological modelling will be, and the easier the lateral seismic interpretation will become. It is hoped that the distribution of petrophysical rock parameters can be estimated in any area of sparse well control, with seismic data as a guide. Therefore, spatial modelling techniques should be used to generate the best geological interpretation and understand the associated uncertainties.

Seismic inversion aims to reconstruct a quantitative model of the Earth's subsurface, by solving an inverse problem based on seismic measurements.[6] Seismic inversion can provide information about the physical properties of the

reservoir rocks and identify the layers of subsurface rocks through the acoustic impedance profile (AI). The value of the acoustic impedance obtained in the inversion process is its value at certain points, whereas what is required is the overall value in the area of interest. We must therefore use a technique to estimate the values in the vertical and lateral directions, and the methods used for this will be geostatistical.

Geostatistical methods are easily useable at low cost, and provide an adequate framework for incorporating exhaustive secondary information (AI seismic inversion data) to improve the estimates of the primary variables (generated from PCA). The present paper makes use of collocated co-kriging to incorporate AI seismic inversion data as secondary information for mapping the values of the petrophysical rock parameters obtained from the application of PCA to well data.

## 2. Materials and Methods

In this study, we split the data processing into two main steps: (i) preparation of the primary data by applying principal component analysis (PCA) to our well data set (log), and (ii) using collocated co-kriging to interpolate that primary data. The aim of the study is to create a distribution map of the hydrocarbon potency by making use of principal component score data, and a seismic inversion "acoustic impedance" horizon map as a secondary data set to apply collocated co-kriging. We use the programs Paradigm 14.0 and Xlstat to help in this research, especially for constructing the map and performing the PCA. A flowchart of the process is shown in ***Figure 1***.

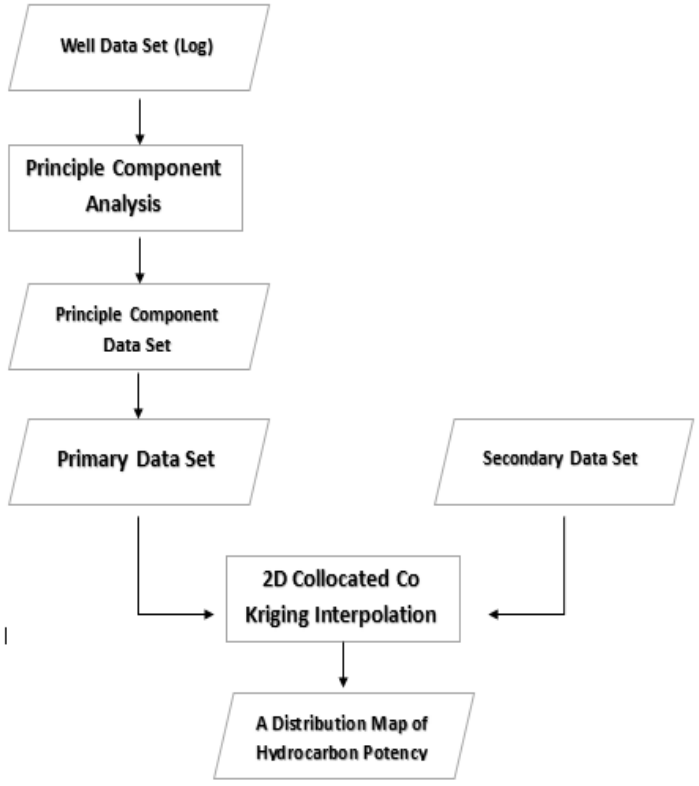


***Figure 1.*** Flow diagram of the process.

*2.1 Well data and principal component analysis*

The physical data that has been compiled from each well is the main source of input data for the principal component analysis (PCA). Principal component analysis (PCA) is a multivariate data dimensionality reduction technique, used to simplify a data set to a smaller number of factors which explain most of the variability (variance).[1]

In this study, there are data from 5 well sites that have deviated mechanisms (i.e., the well is not drilled straight down) with different orientations. The physical characteristics that are used as input values for the PCA are ; GR (Iγ) – total gamma ray intensity [API], RLLD (ρLLD) – dual laterolog deep resistivity [Ω·m], NPHI (ΦN) – compensated neutron porosity [V/V], DEN (δ) – compensated bulk density [g/cm$^3$], and DT (Δt) – compensated sonic transit time [μs/ft].

The depth of the wells is about 1600 meters down from the subsurface. In actual fact, the distribution of well sites in the data acquired by PT Pertamina EP Asset 3 is clustered around the center of the low Acoustic Impedance (AI)-value map. There are four well sites that have been drilled in a specific alignment or orientation with 5-10 meter of spacing between each of them in the center of the AI Map, and one well site on the upper right side (outside the center of the AI map).

The first step toward generating the primary data from the principal component analysis is to produce a correlation matrix between each pair of variables using all the data from the wells in Field X, which we will label X-1, X-2, X-3, X-4, and X-5. Each well that we are using for prospecting has available data logs for five variables (NPHI, DT, RHOB, GR, and ILD). The matrix of correlations for the data from all the wells in Field X is shown in ***Tables 1 - 5***.

***Table 1***. Correlation matrix for well X-1

| Variables | DT | GR | ILD | NPHI | RHOB |
|---|---|---|---|---|---|
| DT | 1 | 0.338 | -0.076 | 0.853 | -0.653 |
| GR | 0.338 | 1 | -0.063 | 0.291 | 0.024 |
| ILD | -0.076 | -0.063 | 1 | -0.110 | 0.026 |
| NPHI | 0.853 | 0.291 | -0.110 | 1 | -0.785 |
| RHOB | -0.653 | 0.024 | 0.026 | -0.785 | 1 |

***Table 2.*** Correlation matrix for well X-2

| Variables | DT | GR | ILD | NPHI | RHOB |
|---|---|---|---|---|---|
| DT | 1 | 0.251 | -0.064 | 0.016 | -0.196 |
| GR | 0.251 | 1 | -0.106 | 0.013 | 0.466 |
| ILD | -0.064 | -0.106 | 1 | -0.001 | 0.035 |
| NPHI | 0.016 | 0.13 | -0.001 | 1 | -0.004 |
| RHOB | -0/196 | 0.466 | 0.035 | -0.004 | 1 |

***Table 3.*** Correlation matrix for well X-3

| Variables | DT | GR | ILD | NPHI | RHOB |
|---|---|---|---|---|---|
| DT | 1 | 0.288 | -0.040 | 0.586 | -0.250 |
| GR | 0.288 | 1 | -0.065 | 0.601 | 0.509 |
| ILD | -0.040 | -0.065 | 1 | -0.098 | -0.041 |
| NPHI | 0.586 | 0.601 | -0.098 | 1 | -0.183 |
| RHOB | -0.250 | 0.509 | -0.041 | -0.183 | 1 |

***Table 4.*** Correlation matrix for well X-4

| Variables | DT | GR | ILD | NPHI | RHOB |
|---|---|---|---|---|---|
| DT | 1 | 0.635 | -0.040 | 0.416 | -0.250 |
| GR | 0.635 | 1 | -0.065 | 0.646 | 0.509 |
| ILD | 0.416 | 0.646 | 1 | -0.098 | -0.041 |
| NPHI | -0.198 | -0.133 | -0.098 | 1 | -0.183 |
| RHOB | 0.142 | 0137 | -0.041 | -0.558 | 1 |

***Table 5.*** Correlation matrix for well X-5

| Variables | DT | GR | ILD | NPHI | RHOB |
|---|---|---|---|---|---|
| DT | 1 | 0.739 | -0.138 | 0.776 | -0.366 |
| GR | 0.739 | 1 | -0.195 | 0.773 | -0.016 |
| ILD | -0.138 | -0.195 | 1 | -0.145 | -0.155 |
| NPHI | 0.776 | 0.773 | -0.145 | 1 | -0.535 |
| RHOB | -0.366 | -0.016 | -0.155 | -0.535 | 1 |

From the correlation matrices, we have extracted the eigenvalues for each of the wells as a second step in performing the PCA. These eigenvalues determine the principal components for each dataset, and more importantly the share of the variance due to each component. In this study, the PCA of the well data for Field X produces 5 separate principal components. The eigenvalues for each of the observed fields are shown in ***Tables 6 - 10***.

***Table 6.*** Eigenvalues for well X-1

| | F1 | F2 | F3 | F4 | F5 |
|---|---|---|---|---|---|
| Eigenvalue | 2.623 | 1.057 | 0.957 | 0.255 | 0.109 |
| Variability | 52.450 | 21.134 | 19.144 | 5.096 | 2.176 |
| Cumulative | 52.450 | 73.584 | 92.728 | 97.824 | 100.000 |

***Table 7.*** Eigenvalues for well X-2

| | F1 | F2 | F3 | F4 | F5 |
|---|---|---|---|---|---|
| Eigenvalue | 1.478 | 1.202 | 1.000 | 0.952 | 0.368 |
| Variability | 29.569 | 24.036 | 19.997 | 19.043 | 7.354 |
| Cumulative | 29.569 | 53.605 | 73.603 | 92.646 | 100.000 |

***Table 8.*** Eigenvalues for well X-3

| | F1 | F2 | F3 | F4 | F5 |
|---|---|---|---|---|---|
| Eigenvalue | 2.011 | 1.448 | 0.985 | 0.441 | 0.116 |
| Variability | 40.220 | 28.957 | 19.693 | 8.816 | 2.313 |
| Cumulative | 40.220 | 69.177 | 88.870 | 97.687 | 100.000 |

***Table 9.*** Eigenvalues for well X-4

| | F1 | F2 | F3 | F4 | F5 |
|---|---|---|---|---|---|
| Eigenvalue | 2.238 | 1.366 | 0.926 | 0.395 | 0.076 |
| Variability | 44.757 | 27.319 | 18.514 | 7.896 | 1.514 |
| Cumulative | 44.757 | 72.077 | 90.590 | 98.486 | 100.000 |

***Table 10.*** Eigenvalues for well X-5

| | F1 | F2 | F3 | F4 | F5 |
|---|---|---|---|---|---|
| Eigenvalue | 2.725 | 1.217 | 0.756 | 0.241 | 0.062 |
| Variability | 54.497 | 24.344 | 15.115 | 4.812 | 1.232 |
| Cumulative | 54.497 | 78.841 | 93.956 | 98.768 | 100.000 |

The eigenvalues for each set of well data yield the corresponding eigenvectors and factor loadings, which will shortly be used to construct the new projected data set. The eigenvalues are determined by **Equation 1**.

$$AV_1 = \lambda V_1 \quad (1)$$

Here, $A$ is any of the correlation matrices, λ is an eigenvalue, and $V_1$ is the corresponding eigenvector. The eigenvalues and loading factors for each well are shown in ***Tables 11 - 15***.

***Table 11.*** Eigenvectors for well X-1

| | F1 | F2 | F3 | F4 | F5 |
|---|---|---|---|---|---|
| DT | 0.570 | 0.026 | 0.081 | 0.683 | -0.449 |
| GR | 0.221 | 0.722 | 0.550 | -0.342 | -0.099 |
| ILD | -0.084 | -0.575 | 0.812 | 0.024 | 0.043 |
| NPHI | 0.595 | -0.046 | -0.014 | 0.034 | 0.802 |
| RHOB | -0.515 | 0.380 | 0.177 | 0.644 | 0.380 |

***Table 12.*** Eigenvectors for well X-2

| | F1 | F2 | F3 | F4 | F5 |
|---|---|---|---|---|---|
| DT | 0.138 | 0.775 | 0.004 | 0.433 | -0.438 |
| GR | 0.735 | -0.167 | -0.003 | 0.119 | 0.646 |
| ILD | -0.133 | -0.412 | 0.187 | 0.876 | 0.098 |
| NPHI | 0.018 | 0.082 | 0.982 | -0.168 | -0.006 |
| RHOB | 0.650 | -0.441 | 0.013 | -0.043 | -0.617 |

***Table 13.*** Eigenvectors for well X-3

| | F1 | F2 | F3 | F4 | F5 |
|---|---|---|---|---|---|
| DT | 0.521 | -0.360 | 0.060 | -0.771 | 0.020 |
| GR | 0.555 | 0.456 | 0.119 | 0.188 | 0.659 |
| ILD | -0.119 | -0.071 | 0.989 | 0.028 | -0.037 |
| NPHI | 0.636 | -0.166 | 0.030 | 0.495 | -0.567 |
| RHOB | 0.040 | 0.793 | 0.053 | -0.352 | -0.492 |

***Table 14.*** Eigenvectors for well X-4

| | F1 | F2 | F3 | F4 | F5 |
|---|---|---|---|---|---|
| DT | 0.507 | 0.367 | -0.001 | 0.780 | -0.006 |
| GR | 0.570 | 0.289 | 0.191 | -0.511 | -0.542 |
| ILD | 0.577 | -0.351 | 0.195 | -0.205 | 0.68 |
| NPHI | -0.245 | 0.088 | 0.958 | 0.119 | 0.015 |
| RHOB | -0.157 | 0.807 | -0.088 | -0.274 | 0.491 |

***Table 15.*** Eigenvectors for well X-5

| | F1 | F2 | F3 | F4 | F5 |
|---|---|---|---|---|---|
| DT | 0.551 | -0.011 | 0.112 | 0.821 | 0.097 |
| GR | 0.512 | -0.294 | 0.416 | -0.332 | -0.606 |
| ILD | -0.125 | 0.685 | 0.715 | -0.012 | 0.061 |
| NPHI | 0.578 | 0.086 | -0.046 | -0.460 | 0.667 |
| RHOB | -0.290 | -0.661 | 0.548 | 0.062 | 0.418 |

***Table 16.*** Factor loadings for well X-1

| | F1 | F2 | F3 | F4 | F5 |
|---|---|---|---|---|---|
| DT | 0.923 | 0.027 | 0.080 | 0.345 | -0.148 |
| GR | 0.358 | 0.743 | 0.538 | -0.173 | -0.033 |
| ILD | -0.084 | -0.575 | 0.812 | 0.024 | 0.014 |
| NPHI | 0.595 | -0.046 | -0.014 | 0.034 | 0.264 |
| RHOB | -0.515 | 0.380 | 0.177 | 0.644 | 0.125 |

***Table 17.*** Factor loadings for well X-2

| | F1 | F2 | F3 | F4 | F5 |
|---|---|---|---|---|---|
| DT | 0.168 | 0.850 | 0.004 | 0.423 | -0.266 |
| GR | 0.894 | 0.183 | -0.003 | 0.116 | 0.392 |
| ILD | -0.162 | -0.452 | 0.187 | 0.855 | 0.059 |
| NPHI | 0.022 | 0.089 | 0.982 | -0.164 | -0.004 |
| RHOB | 0.790 | -0.484 | 0.013 | -0.042 | -0.374 |

***Table 18.*** Factor loadings for well X-3

| | F1 | F2 | F3 | F4 | F5 |
|---|---|---|---|---|---|
| DT | 0.739 | -0.433 | 0.059 | -0.529 | 0.007 |
| GR | 0.787 | 0.549 | 0.118 | 0.125 | 0.224 |
| ILD | -0.169 | -0.085 | 0.982 | 0.018 | -0.013 |
| NPHI | 0.902 | -0.200 | 0.030 | 0.329 | -0.193 |
| RHOB | 0.057 | 0.955 | 0.053 | -0.234 | -0.167 |

***Table 19.*** Factor loadings for well X-4

| | F1 | F2 | F3 | F4 | F5 |
|---|---|---|---|---|---|
| DT | 0.759 | 0.429 | -0.001 | 0.490 | -0.002 |
| GR | 0.853 | 0.337 | 0.184 | -0.321 | -0.149 |
| ILD | -0.366 | 0.103 | 0.922 | 0.075 | 0.004 |
| NPHI | 0.863 | -0.410 | 0.187 | -0.129 | 0.187 |
| RHOB | -0.235 | 0.943 | -0.084 | -0.172 | 0.135 |

***Table 20.*** Factor loadings for well X-5

| | F1 | F2 | F3 | F4 | F5 |
|---|---|---|---|---|---|
| DT | 0.910 | -0.012 | 0.097 | 0.403 | 0.024 |
| GR | 0.845 | -0.324 | 0.362 | -0.163 | -0.150 |
| ILD | -0.206 | 0.755 | 0.622 | -0.006 | 0.015 |
| NPHI | 0.954 | 0.095 | -0.040 | -0.226 | 0.165 |
| RHOB | -0.479 | -0.730 | 0.476 | 0.030 | 0.104 |

The transformation of the primary data into a projected data set by making use of the information about the components is a critical step in PCA. The multivariate information carried by the primary data acts as input data for the next step in the process. This multivariate information will provide fundamental guidance for the interpretation of the interpolated data map that will result from the collocated co-kriging.

In this study, we will choose a principal component that has a high loading factor for the variables GR, NPHI, and DT. For this reason, we stipulate that for wells X-1, X-3, X-4, and X-5 we will be using Component 1 (F1) and for well X-2 Component 2 (F2). The purpose of this selection is to allow us to interpolate the primary data while retaining information about the porous rock stratum and the hydrocarbon (gas or oil) potency.

After calculating the eigenvectors for each set of well data and selecting single components, the next step is to construct a new data set called the principal component scores (PCS). It should be noted that the PCS is a projected data set that carries information about the primary data and is built from the factor loadings. The values of the PCS for each well are shown in ***Tables 21 – 25***.

***Table 21.*** Principal component scores for well X-1

| Observation | F1 | F2 | F3 | F4 | F5 | DEPTH |
|---|---|---|---|---|---|---|
| Obs1 | 2.54 | -0.269 | -0.103 | 0.339 | 1.302 | 974.286 |
| Obs2 | 2.38 | -0.27 | -0.123 | 0.135 | 1.532 | 974.438 |
| Obs3 | 2.24 | -0.30 | -0.156 | -0.048 | 1.586 | 974.59 |
| Obs4 | 2.26 | -0.46 | -0.467 | -0.244 | -0.356 | 974.743 |
| … | … | … | … | … | … | … |

***Table 22***. Principal component scores for well X-2

| Observation | F1 | F2 | F3 | F4 | F5 | DEPTH |
|---|---|---|---|---|---|---|
| Obs1 | 1.871 | 0.138 | 0.046 | 0.445 | -2.379 | 1122.115 |
| Obs2 | 0.467 | 1.669 | 0.018 | 0.789 | -0.960 | 1122.267 |
| Obs3 | 0.390 | 1.921 | 0.018 | 0.874 | -0.785 | 1122.42 |
| Obs4 | 0.285 | 2.399 | 0.013 | 1.085 | -0.722 | 1122.572 |
| … | … | … | … | … | … | … |

***Table 23.*** Principal component scores for well X-3

| Observation | F1 | F2 | F3 | F4 | F5 | DEPTH |
|---|---|---|---|---|---|---|
| Obs1 | 3.659 | -3.914 | 0.246 | -5.055 | -0.065 | 1148.012 |
| Obs2 | 3.456 | -4.394 | 0.236 | -5.695 | 0.344 | 1148.165 |
| Obs3 | 3.574 | -2.751 | 0.412 | -6.916 | -0.605 | 1148.317 |
| Obs4 | 3.575 | -2.437 | 0.523 | -7.292 | -0.678 | 1148.47 |
| … | … | … | … | … | … | … |

***Table 24.*** Principal component scores for well X-4

| Observation | F1 | F2 | F3 | F4 | F5 | DEPTH |
|---|---|---|---|---|---|---|
| Obs1 | -2.069 | -1.728 | -0.748 | 0.325 | -0.439 | 1533.144 |
| Obs2 | -2.065 | -1.833 | -0.732 | 0.281 | -0.443 | 1533.296 |
| Obs3 | -2.241 | -2.114 | -0.706 | -0.092 | -0.326 | 1533.449 |
| Obs4 | -2.139 | -2.232 | -0.670 | -0.094 | -0.298 | 1533.601 |
| … | … | … | … | … | … | … |

***Table 25.*** Principal component scores for well X-5

| Observation | F1 | F2 | F3 | F4 | F5 | DEPTH |
|---|---|---|---|---|---|---|
| Obs1 | 1.425 | 3.082 | -3.025 | -2.855 | -0.427 | 1593.189 |
| Obs2 | 1.589 | 2.989 | -2.884 | -2.428 | 0.146 | 1593.342 |
| Obs3 | 1.331 | 2.847 | -2.718 | -2.291 | 0.331 | 1593.494 |
| Obs4 | 0.948 | 2.889 | -2.775 | -2.524 | -0.480 | 1593.647 |
| … | … | … | … | … | … | … |

The conditioning step for the primary data is now complete.

*2.2 Acoustic impedance map and collocated co-kriging*

In this study, we use the map of the acoustic impedances of the Z-14 horizons in Field X, which provides an indication of the potential presence of hydrocarbon fluids. This field is located in the West Java Basin, in the Cibulakan Atas formation, which consists of a combination of shale, sandstone, and limestone (see ***Figure 2***).

The AI map that we make use of, as a secondary data set when applying the process of collocated co-kriging, has a spatial extent of 1440 x 2750 $m^2$. Collocated co-kriging is a variant of full co-kriging, where secondary data used for estimation are reduced so as to retain only the secondary datum in the location where the primary variable is being estimated.[4,7] The Z-14 horizon is located at around 1600 m depth, with a variable AI score ranging from 7000 rayl to 10,000 rayl in each sector of the map (as can be seen in the color bar of the AI map in ***Figure 4***). The inversion AI data for the Z-14 horizon of Field X that we use to perform the collocated co-kriging is the property of PT Pertamina EP Asset 3. It was produced by model-based inversion theory (see ***Figure 3***).

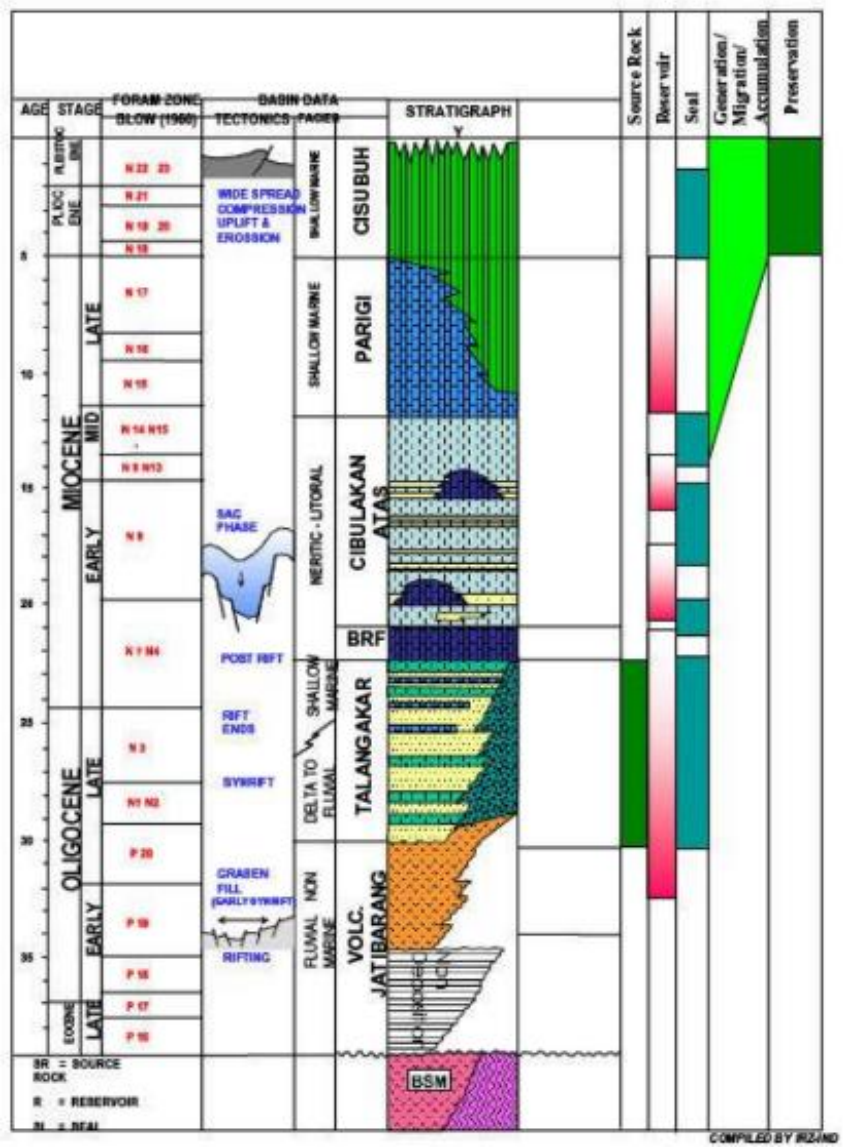


***Figure 2.*** Stratigraphy of West Java Basin[2]

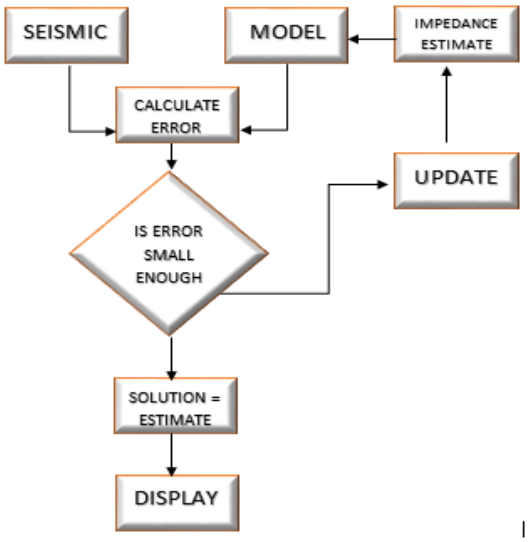


***Figure 3.*** Flow diagram of model-based inversion method

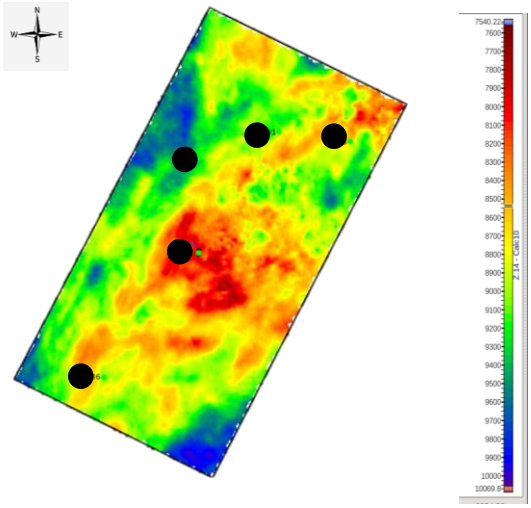

***Figure 4.*** Map of the acoustic impedance with the distribution of PCS for the primary data (black dots)

Based on the given information about the acoustic impedance of the Z-14 horizon, it is clear that there is a low value of the acoustic impedance in the center and upper right of the map. The variable scores can be interpreted as being due to the presence of a porous (not compacted) rock stratum in Field X that contains fluids. This particular data set is one of the considerations that led PT Pertamina EP Asset 3 to decide to make some delineations and collect well log data at several locations, as there was a high probability of a hydrocarbon prospect there.

As mentioned above, the intention is to apply collocated co-kriging to interpolate the values of the PCS extracted from the well log data. Remembering that the well sites deviate from the vertical with different orientations, the intersections of the wells and the Z-14 horizon have different depths on the AI map. So in this case, the PCS at the intersections between the wells and the Z-14 Horizon (at the depth of the horizon) are taken as input data (see ***Figure 5*** and ***Table 26***).

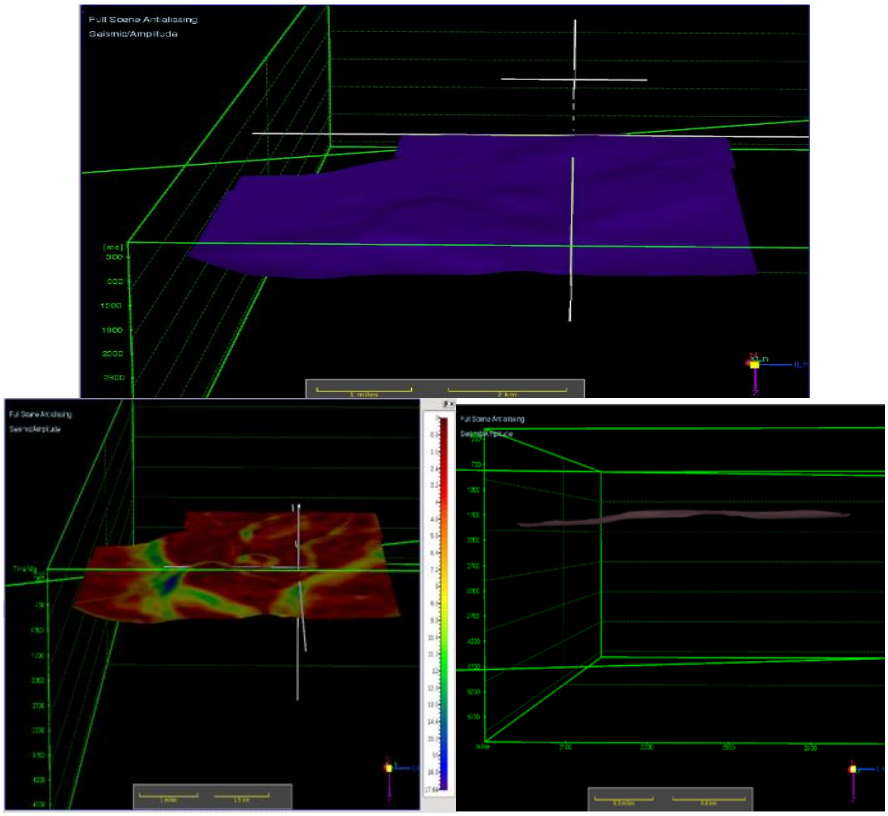

***Figure 5.*** The horizon map of Field X

***Table 26.*** The Primary Data Input from the PCS

| No Well | Depth | PC Score |
|---|---|---|
| X-1 | 1669.31 | 3.921 |
| X-2 | 1665.66 | -0.22 |
| X-3 | 1687.51 | 1.345 |
| X-4 | 1696.2 | 1.301 |
| X-5 | 1657.64 | 1.631 |

The data from the available results of the PCS are used as primary input, and the AI seismic inversion map as densely sampled secondary input data. In addition, to improve the interpolation accuracy, the correlation between the primary and secondary variables should be as high as possible. Therefore we must construct a cross plot between both sets of data.

The red dots in ***Figure 6*** correspond to data sampled from the primary and secondary variables, which have a correlation factor of about -0.765. The cross plot is used to measure the strength of the relationship between the two variables. A negative correlation means that as the value of one variable increases, the other decreases.

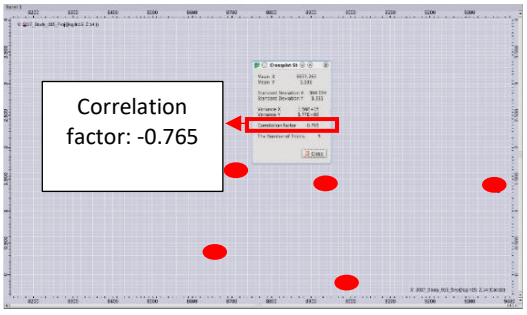


***Figure 6.*** Correlation factor

Collocated co-kriging represents the spatial relationship of the control data in the form of a variogram such as ***Figure 7***. Two important criteria that show the consistency of the spatial structure are the range and the relative nugget effect (nugget effect/sill: *C*0/*C*). The variogram that is more appropriate has a greater range and smaller nugget effect. The variogram below has no nugget effect, with a range of 1218.28 and a sill of 2.53.

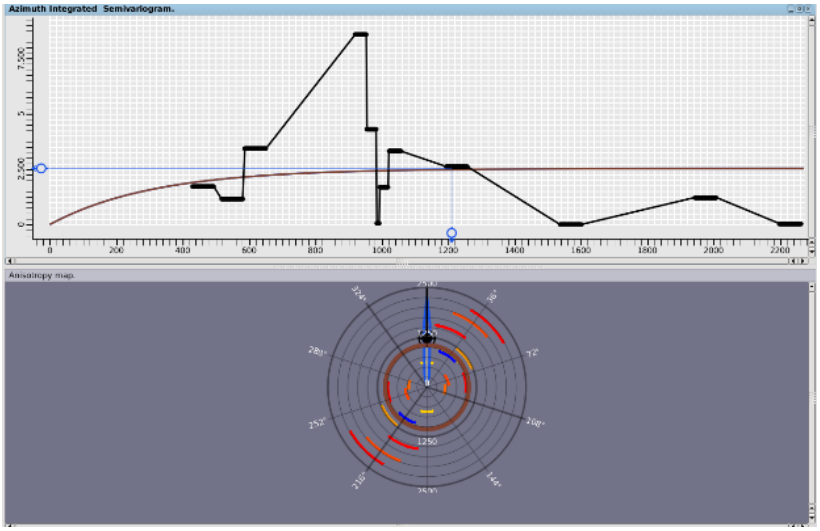


***Figure 7.*** Collocated co-kriging variogram

## 3. Results

Based on the processed output data from Field X, there is a significant hydrocarbon potency in the field, but not at every spot that wasn't sampled. The magnitude of the hydrocarbon potency at each interpolated spot can be examined quantitatively using the color-bar of the map in ***Figure 8***.

The red color intervals are in the range 2.8-3.5 (dimensionless), which can be considered as areas of potential hydrocarbon content having high PCS values. All of the interpolated data, as stated before, refers to the primary data, reduced to principal component Scores (PCS) which contain "multivariate (many variables) information". The variables that contribute to this particular PCS, in this study, are NPHI, GR, and DT. These three variables coherently give information about the presence, or not, of hydrocarbon fluid content and tend to indicate porosity.[3]

The Wyllie formula for calculating sonic porosity can be used to determine porosity in consolidated sandstones and carbonates with intergranular porosity (grainstone) or intercrystalline porosity (sucroise dolomites).[2] Meanwhile, NPHI can be used to calculate vuggy or fracture secondary porosity in carbonates by comparing it to the total porosity. The fracture secondary porosity is found by subtracting the sonic porosity from the total porosity. The Wyllie equation reads:

$$\emptyset_{sonic} = \left(\frac{\Delta t_{log} - \Delta t_{ma}}{\Delta t_f - \Delta t_{ma}}\right) \times 1/Cp \qquad (2)$$

where

$\emptyset_{sonic}$ = sonic derived porosity
$\Delta t_{ma}$ = interval transit time of the matrix
$\Delta t_{log}$ = interval transit time of formation
$\Delta t_f$ = interval transit time of the fluid in the well bore
(fresh mud = 189; salt mud = 185)
$Cp$ = compaction factor

The compaction factor can be calculated from the formula:

$$Cp = \frac{\Delta t_{sh} \times C}{100} \qquad (3)$$

where

$\Delta t_{sh}$ = interval transit time for adjacent shale
$C$ = a constant which is normally[5] 1.0

It can clearly be seen that the high PCS are in general located in the center, left, and lower right corner of the map in ***Figure 8***. These results are completely different from the hydrocarbon potency for Field X predicted from the quantitative values of the acoustic impedance.

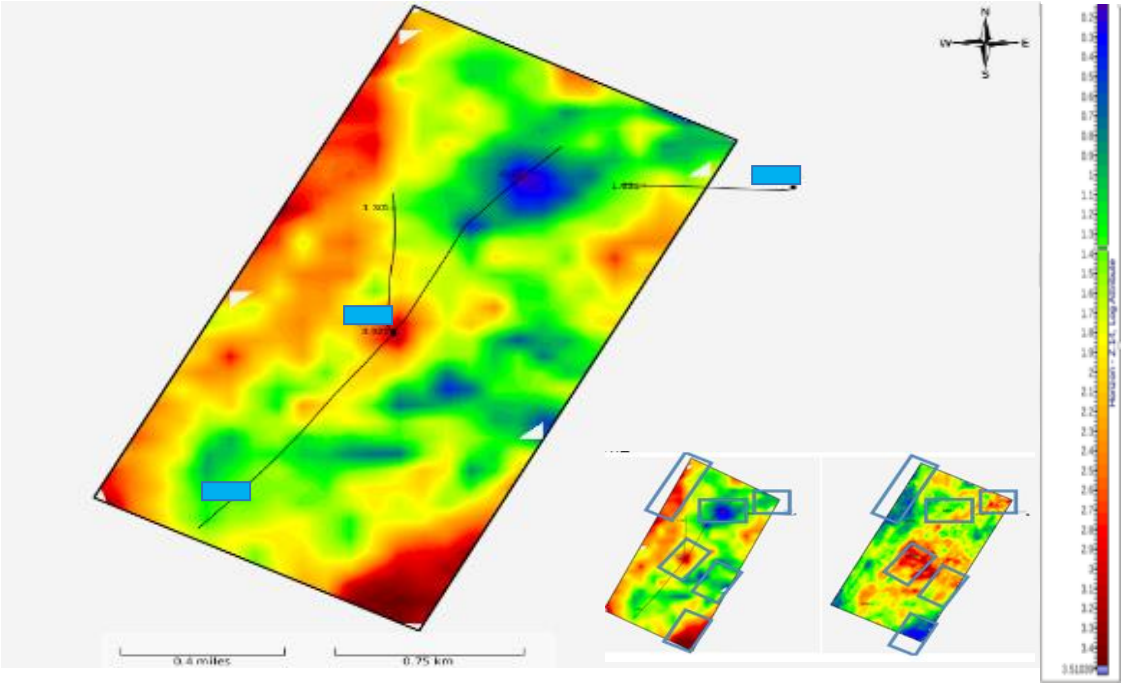

***Figure 8.*** A distribution map of the hydrocarbon potency generated by collocated co-kriging

## 4. Discussion and Conclusion

Here we identify six different zones in the potency map generated by our analysis, which would need some detailed exploration to reveal the accuracy of our hydrocarbon prospecting. It can be positively stated that low values of the AI (red color) for the Z-14 horizon of Field X, should not be regarded as an infallible indicator of hydrocarbon potency in all cases. Our study is based on the application of collocated co-kriging to interpolate the PCS data from all the wells in Field X. Our study simply adds extra information to what is already known about the potency of hydrocarbon discovery at the site, building the AI score, and the interpolated PCS map can be worthwhile as a controlling or enhancing factor if and when it is decided to drill further prospect delineation wells.

In this study, we have performed a quantitative and qualitative test to determine whether the PCS interpolated map is scientifically and intuitively adequate for hydrocarbon prospecting. The quantitative test that we came up was to construct a "cross-plot" section between the primary and secondary data, as shown in ***Figure 6***. The cross-plot in this case has a correlation factor about -0.765 which is close to -1. This indicates a strong relationship between the two data sets. Moreover, the fact that the correlation factor is negative, in this case, signals a reverse relationship between the PCS and the AI seismic inversion data.

Now that the PCS have been interpolated by collocated co-kriging, we continue our interpretation by examining well X-1, which is located at the center of our output map in ***Figure 9.*** This well intersects the Z-14 horizon in the red colored zone on the output map. We also have data from Pertamina EP Asset 3 that gives us information about the gas production from this well (see ***Figure 10***). This information allows us to extend our predictions to gas potency in the area, which is highest in the red colored zones in an output map very similar to ***Figure 9.*** Even though we are predicting that most of the red-colored zones have high gas potency, we are not recommending HD3 because that zone is located relatively far from all the sampled wells.

What about the blue colored zones in ***Figure 9***? We can also make some predictions for those zones. As a starting point for these predictions, we use the production performance data we have for well X-2. In this well, the production is dominated by oil

(see ***Figure 11***). In view of this, we have identified 5 blue zones in ***Figure 12*** that we expect to have high oil potency, although more detailed exploration would be needed to test the accuracy of this hydrocarbon prospecting**.**

We can also perform a qualitative validation of the accuracy of the combined PCA and collocated co-kriging results by estimating the hydrocarbon potency in an un-sampled area. As we stated before, all the well data and the acoustic impedance map used in this study are the property of PT Pertamina EP Asset 3. The total data set from Field X includes data from a sixth well. We can therefore perform a validation of the PCS map generated in this study by using all the well data for Field X. We have used the data from the first five well (X-1, X-2, X-3, X-4, and X-5) to predict the hydrocarbon potency in Field X, and the validation data comes from the sixth well (X-6). The validation data from X-6 is shown in the production performance graph for the Z-14 horizon in ***Figure 13***.

Based on the wells location data we have for the Z-14 Horizon, well X-6 is located in zone HD1 (see ***Figure 9*)**. In any case, a comprehensive further geological and geophysics analysis is needed for zones HD2, HD3, HD4, and RBA1-RBA5 to check the potential presence of hydrocarbons.

Moreover, it can be concluded that the PCS distribution map generated from the combined PCA-collocated co-kriging method has successfully mapped the hydrocarbon potency as a guide for more detailed exploration in Field X.

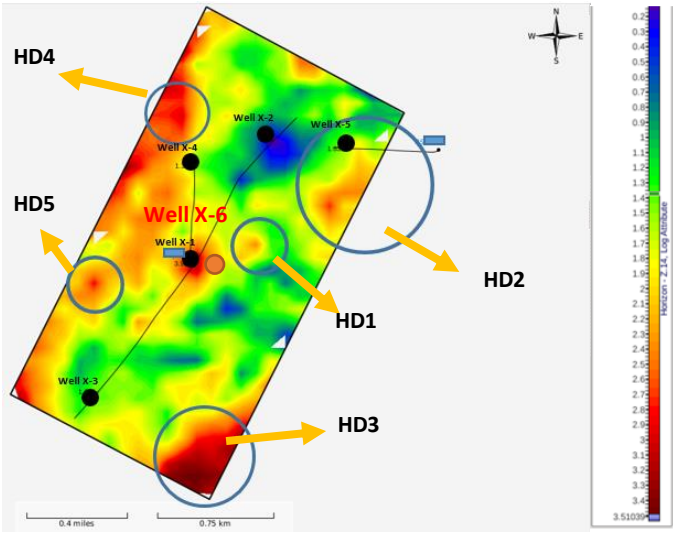


***Figure 9.*** Six different zones in the distribution map with high hydrocarbon potency generated by the collocated co-kriging and the acoustic impedance map

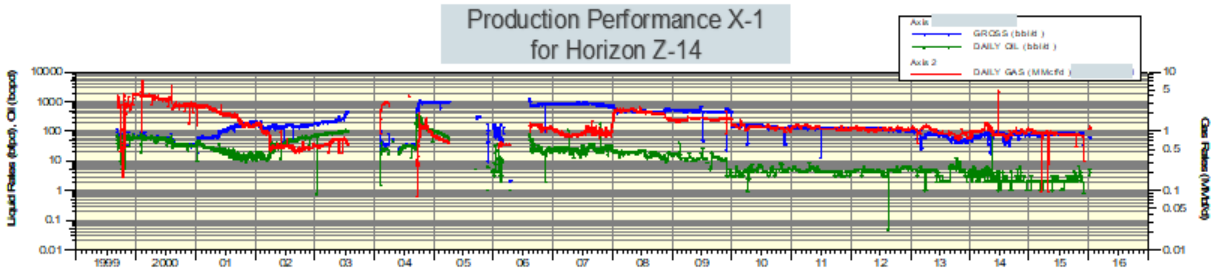


***Figure 10.*** Production performance for Well X-1

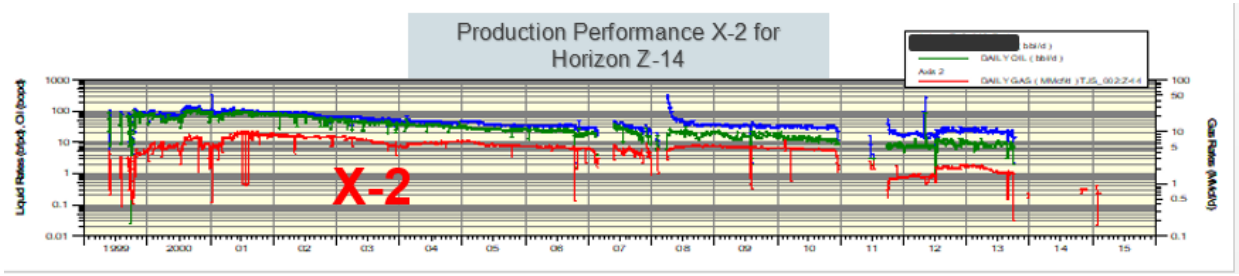


***Figure 11.*** Production performance for Well X-2

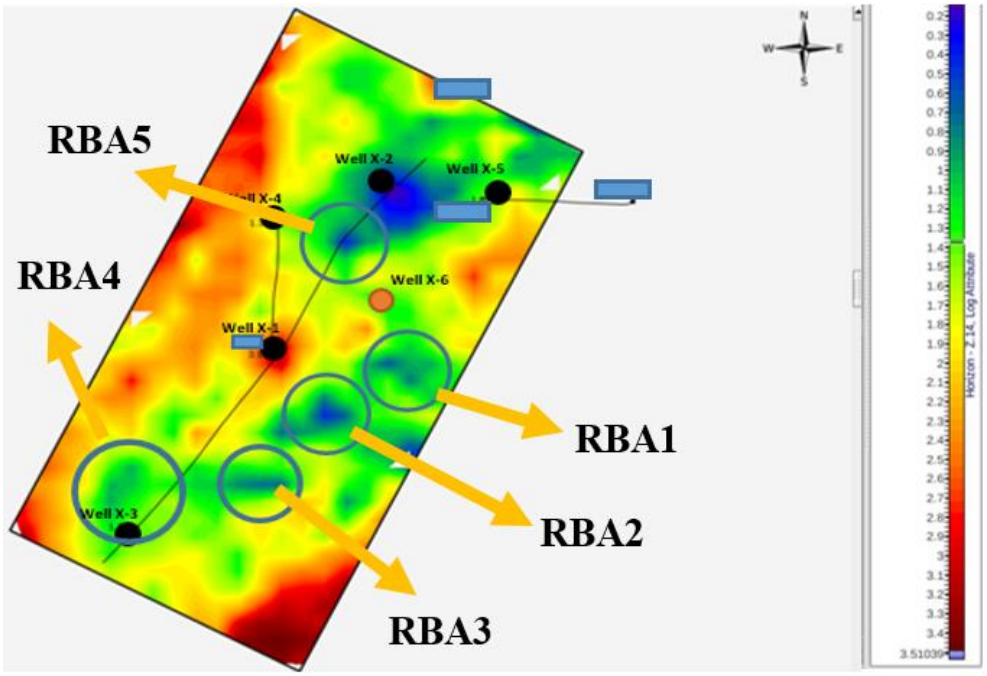


***Figure 12.*** Blue colored zones predicted to have high oil potency

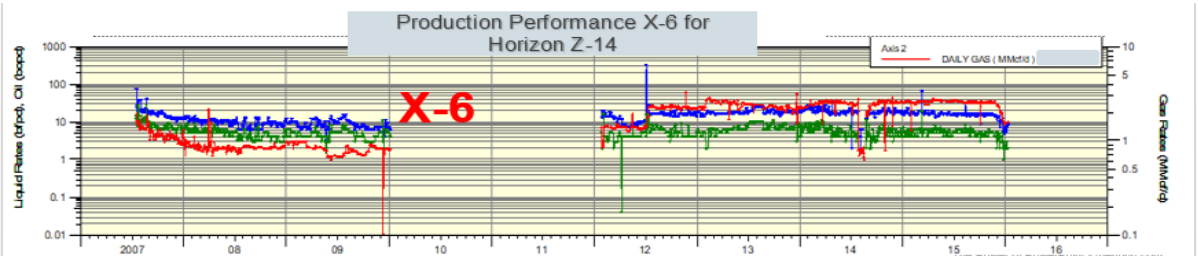


***Figure 13***. Production performance of well X-6 (upper) for the Z-14 horizon.

**Acknowledgements**

We would like to extend our sincere gratitude to PT Pertamina EP Asset 3, especially to Mr Dias Pramudito and Mr Andreas Wasi for their help and support in using their data and software. Thanks also to our beloved lecturer, Ms Susasnti Alawiyah in Bandung Institute of Technology for her assistance, guidance and support in all phases of this study.

**References**

[1] G. Andrei and B. M. Niculescu, "Principal component analysis as a tool for enhanced well log interpretation", *Geoscience 2016*.

[2] D. Arpandi and S. Patmokismo, "The Cibulakan Formation as one of the most prospective stratigraphic units in the north-west Java basinal area", *IPA Proceedings*, **1975**, 181-210.

[3] G. Asquith and C. Gibson, *Basic Well Log Analysis for Geologists: Methods in Exloration Series*, American Association of Petroleum Geologists, **1982**, Tulsa, Oklahoma.

[4] M. N. M. Boezio, J. F. C. L. Costa and J. C. Koppe, "Kriging with an external drift versus collocated co-kriging for water table mapping", *Applied Earth Science*, **2006**, 115(3), 103-112.

[5] D. W. Hilchie, *Applied Openhole Log Interpretation for Geologists and Petroleum Engineers*, Colorado School of Mines, **1978**.

[6] Y. Wang, *Seismic Inversion: Theory and Applications*, **2016**, John Wiley and Sons.

[7] W. Xu, T. Tran, R. M. Srivastava, and A. G. Journel, "Integrating seismic data in reservoir modelling: the collocated co-kriging alternative", *SPE annual technical conference and exhibition*, **1992**, Society of Petroleum Engineers.

# SCIENTIA BRUNEIANA

# NOTES TO CONTRIBUTORS

**Manuscript Submission and Specifications**

***Scientia Bruneiana*** is published twice a year. The deadline for submission of manuscripts is **30th June for the end of year edition** and the **31st December for the May edition**.

Manuscripts should be submitted in Microsoft Office Word (.DOCX) format to the Scientia Bruneiana website, at https://scibru.fos.ubd.edu.bn.

Papers will be refereed prior to acceptance. Authors are welcome to suggest potential international referees.

Articles outlining original research findings as well as mini-review articles are welcomed. There are two special categories: "Brief Communications" and "Research Notes". Contributions to either category should be 300 to 1000 words long (no more than 3 pages in length). The "Research Notes" section is earmarked for summaries of the results and outcomes of projects receiving UBD Science Faculty research grants.

Manuscripts should be written in English (British or American). All manuscripts should be in 12pt Times New Roman, **single-spaced**, **single column** and A4 formatted (2cm margins from the edge).

**Title page**

The first page should include the title of the article, author's names and addresses of the institutions involved in the work. The paper title is only capitalized on proper nouns and the first letter. Latin, scientific genus and species should be italicized. The authors' affiliations are denoted with a superscripted number and the corresponding author denoted with a * at the end of the author's name. Only the corresponding author's email need to be listed.

Example format of the title page:

## First record and conservation value of *Periophthalmus malaccensis* Eggert from Borneo

*First Author[1*], John H. Smith[2,3], Muhamad Ali Abdullah[2] and Siti Nurul Halimah Hj. Ahmad[1]*

*[1]Environmental and Life Sciences, Faculty of Science, Universiti Brunei Darussalam, Jalan Tungku Link, Gadong, BE1410, Brunei Darussalam*
*[2]Department of Chemical Sciences, Faculty of Science, Universiti Brunei Darussalam, Jalan Tungku Link, Gadong, BE1410, Brunei Darussalam*
*[3]Department, University, Street Adress, Postcode, Country*

**corresponding author email: corresponding.author@ubd.edu.bn*

**Abstract Page and Index Terms**

The second page of the manuscript should include the abstract (up to 300 words) and index terms (subject heading, or descriptor, in information retrieval, that captures the essence of the topic of a document).

Example format of the abstract and index terms page:

### Abstract

The abstract is a self-contained description of the work in one paragraph of up to 300 words. It must include no references or foot notes, but it must describe the key points of the work. This should include

a description of the work that was done and why it was it done. It should include brief conclusions and any significant numerical findings such as derived constants or important parameters.

*Index Terms:* resolution, spectroscopy, microscopy

**Main body of text**

For original research articles, the main body of text of the manuscript should include the following appropriately numbered sections: **1. Introduction**, **2. Experimental approach**, **3. Results and Discussions** and **4. Conclusion** followed by **Acknowledgements**, **References** and **Appendices** (if necessary).

Each different numbered section may contain italicised subheadings which are numbered appropriately, e.g. *2.1*, *3.1*, etc.

Review articles will obviously not conform to this format. In the case of other submissions where the above format may be unsuitable, you are advised to contact the editor prior to submitting the article.

*Reference to figures, tables and equations*

The main body of text should not include figures and/or tables, but should refer to figures and tables. If a certain figure or table was not referred to in the main body of text then it will be considered irrelevant and therefore will not be included in the publication. When referring to a figure or table in the text, the words figure and/or table should be bold and italicized e.g. ***Figure 1*** and ***Table 1***. The words "figure" and "table" should be spelled out in full and not abbreviated. For further instructions on figures and tables (including dimensions, colour schemes and formats), please refer to the figures and tables section (below).

Equations could be displayed in-line or centred by itself, but must be accompanied by a number and individual terms/symbols explained. When When referring to the equation in the text, the word "Equation" should be bold and italicized e.g. ***Equation 1***. The words "Equation" should be spelled out in full and not abbreviated.

Example format of equation:

An example of an equation is shown for ***Equation 1***, Weber Morris intraparticle diffusion:

$$q_t = k_{id} t^{1/2} + C \qquad (1)$$

and Boyd model (***Equation 2***):

$$F = 1 - \frac{6}{\pi^2} exp(-B_t) \qquad (2)$$

where F = $q_t$ / $q_e$, $F$ is the fraction of solute adsorbed at any time, $t$ and $B_t$ is mathematical function of $F$.

*In-line citation style*

The in-line citation should be in IEEE referencing format (numbers with square brackets), generated using a reference manager. Example:

> Even though various studies have shown this [1]–[5], there are others that have contradicted this [6]–[10]. Data was obtained from [11].

Please note that brackets should go **before** punctuation.

*References*

The reference/bibliographic list should only include references cited in the text and should be listed in the references section in the following format:

> Journal article
> [1] J. H. Surname and J. E. Doe, "Title," *Journal*, Vol., No., Pages, Year. DOI: (number)

Textbook/Chapter of a book
[2] J. H. Surname and J.E. Doe, *Title of Textbook*, Publication House, Year.

Dissertation/Thesis
[3] J.H. Surname, "Title of Thesis," University, Year

Webpages/Online Databases
[4] "Website/Database name/body," Year. Available: http;//www.weburl.com. [Accessed 18-Apr-2017]

These should be generated automatically if a reference manager software has been used. When there are **three or more authors**, just state the name of the first author, e.g. J. H. Surname, et. al. Please include the digital object identifier (DOI) for journal articles.

**Figures and Tables**

A list of tables, figures and captions should be given at the end of the manuscript after the reference list. These must be appropriately numbered in the order that they appear in the paper. Each table and figure must be adequately discussed and referenced in the text. It is important that you do not include tables and figures in the main body of text of your submitted manuscript.

*Sizing*

Please keep tables/figures/images/illustrations to have a **maximum width of either 8.4 cm (single column) or 17.5 cm (double column)**, with enough clarity that the images does not appear blurred, skewed or pixelated (unless the pixelation is unavoidable from the raw data collection).

*Text*

Texts in figures and tables should be 10pt, using either Times New Roman, Arial or Calibri font, with consistent font size and style throughout the manuscript's figures/tables/artwork/images/illustrations. Please ensure that texts do not fall below 8pt size as this will greatly affect readability of said text.

*Colour*

Colour images are highly encouraged for the on-line issue, however they should be designed such that the information is still obvious in grey-scale too for the print version.

*Graphs*

Graphs could either be saved as an embedded graph format in DOCX or as an image (JPEG or TIFF). Graphs should have clearly-labelled axes and lines that can be distinguished in both color for on-line and grey-scale for print version. You can use dotted and dashed lines etc, or you can use different data point types when appropriate to discriminate between data sets.

*Tables*

Tables could either be saved as an embedded table format in DOCX or as an image (JPEG or TIFF), with appropriate captions/titles.

*Captions*

All figures and tables should be appropriately captioned. The caption should be sufficiently able to explain the figure/table without the reader having to refer to the main text. The words "figure" and/or "table" should be bold. italicized and spelled out fully (not abbreviated), followed by a full stop (also bold and italicized). The rest of the caption should not be bold and italicized (unless it is a scientific genus or species).

Example format for figure/table caption:

> ***Figure 1.*** *Periophthalmus malaccensis* collected in Sungai Bunga, Brunei (UBDM MBu081013mal); a. freshly dead specimen, lateral view; b. live specimen; c. freshly dead specimen, ventral view, detail (scale bars are 10 mm long).

**Manuscripts that do not conform to the above instructions will be returned without review.**